plants

MDPI

Article

Coupled Gas-Exchange Model for C_4 Leaves Comparing Stomatal Conductance Models

Kyungdahm Yun [1], Dennis Timlin [2] and Soo-Hyung Kim [1,*]

[1] School of Environmental and Forest Sciences, College of the Environment, University of Washington, Seattle, WA 98195, USA; kdyun@uw.edu

[2] Adaptive Cropping Systems Laboratory, Agricultural Research Service, U.S. Department of Agriculture, Beltsville, MD 20705, USA; dennis.timlin@usda.gov

* Correspondence: soohkim@uw.edu

Received: 31 August 2020; Accepted: 4 October 2020; Published: 14 October 2020

Abstract: Plant simulation models are abstractions of plant physiological processes that are useful for investigating the responses of plants to changes in the environment. Because photosynthesis and transpiration are fundamental processes that drive plant growth and water relations, a leaf gas-exchange model that couples their interdependent relationship through stomatal control is a prerequisite for explanatory plant simulation models. Here, we present a coupled gas-exchange model for C_4 leaves incorporating two widely used stomatal conductance submodels: Ball–Berry and Medlyn models. The output variables of the model includes steady-state values of CO_2 assimilation rate, transpiration rate, stomatal conductance, leaf temperature, internal CO_2 concentrations, and other leaf gas-exchange attributes in response to light, temperature, CO_2, humidity, leaf nitrogen, and leaf water status. We test the model behavior and sensitivity, and discuss its applications and limitations. The model was implemented in Julia programming language using a novel modeling framework. Our testing and analyses indicate that the model behavior is reasonably sensitive and reliable in a wide range of environmental conditions. The behavior of the two model variants differing in stomatal conductance submodels deviated substantially from each other in low humidity conditions. The model was capable of replicating the behavior of transgenic C_4 leaves under moderate temperatures as found in the literature. The coupled model, however, underestimated stomatal conductance in very high temperatures. This is likely an inherent limitation of the coupling approaches using Ball–Berry type models in which photosynthesis and stomatal conductance are recursively linked as an input of the other.

Keywords: gas-exchange; C_4 photosynthesis; stomatal conductance; Ball–Berry; Medlyn

1. Introduction

Leaf gas-exchange includes the processes of CO_2 assimilation and water vapor exchange by plant leaves. It is one of the most important processes for life on Earth as it provides carbohydrate for food and oxygen for respiration practically for all organisms. Because plant growth depends on photosynthesis, it is an essential building block of plant simulation models. Photosynthesis models range in complexity from correlative models based on radiation use efficiency where carbon assimilation is proportional to total irradiance absorbed by leaf surfaces, to models based on enzyme kinetics [1]. Integration of more mechanistic photosynthesis model has been a critical aspect in crop modeling to better understand and predict crop productivity under dynamic environments [2,3].

A coupled approach to modeling photosynthesis, stomatal conductance, and transpiration simultaneously for C_3 plants has been presented by a number of studies [4–8]. This approach usually combines the FvCB (Farquhar–von Caemmerer–Berry) C_3 photosynthesis model [9] with a model of

stomatal conductance [5,10,11] and an energy balance equation. The coupled modeling approach can describe the photosynthetic behavior of leaves by taking into account the biochemical limitation for CO_2 assimilation (demand), as well as the stomatal and other biophysical limitations in CO_2 supply, linked to transpiration and leaf temperature. These models describe photosynthesis mechanistically based on its key biochemical and anatomical characteristics.

Similarly to the C_3 model, a simplified biochemical model is also available for C_4 photosynthesis that takes into account CO_2 concentrating mechanism with the anatomical and functional separation between the mesophyll and bundle sheath cells [12]. However, while a number of studies have adapted and applied the coupled modeling approach for C_3 leaves, its application in C_4 leaves has been limited, with few exceptions [13,14]. An open source implementation of coupled gas-exchange modeling in R language is available with an emphasis on C_3 leaves [15]. A photosynthesis model with an emphasis on plant hydraulic balance of crassulacean acid metabolism (CAM) plants is available in Python language [16]. Dynamic programming languages, such as Python and R, are often easier to use in an interactive session, but suffer from slow performance. Julia is a new dynamic programming language primarily designed for the use in scientific computing with performance in mind [17].

Leaf gas-exchange processes can be limited by internal and external stress factors, such as leaf nitrogen and soil water availability [18]. A process-based model should incorporate these stress responses for realistic representation of the leaf gas-exchange processes. Correlations between key enzymatic parameters and leaf nitrogen content were often derived to describe down-regulation of photosynthesis under non-optimal nitrogen availability [19–21]. Stomatal conductance submodel was extended to acknowledge soil water status via leaf water potential and control the amount of transpiration and associated photosynthetic activity [20,22,23].

Meanwhile, many existing coupled photosynthesis models have relied on an empirical relationship between photosynthesis and stomatal behavior as established by Ball, Woodrow, and Berry, often referred to as Ball–Berry model [10]. Medlyn model extended Ball–Berry model in a similar structure to provide a better theoretical interpretation [11]. Comparisons between the two models generally reported similar performance when compared under usual conditions [24,25].

In this study, we developed a coupled gas-exchange model for C_4 leaves to compare performance of two stomatal conductance models: Ball–Berry (BB) and Medlyn (MED). Simulation using the two variants of coupled model were carried out under multiple environmental conditions with a varying degree of humidity, CO_2 concentration, air temperature, and irradiance. Responses to the simultaneous application of nitrogen and water stress were also investigated. Only a small number of model parameters were calibrated to an observation dataset, while most parameter values were from existing literature and models. An application of the model to replicate a known experiment with transgenic plants under a range of temperature is also discussed.

2. Results

2.1. Gas-Exchange Model Calibration

The performance of calibrated parameters was evaluated by Willmott's refined index of agreement (d_r) and Nash–Sutcliffe model efficiency coefficient (NSE) for the two variants of gas-exchange model (Figure 1). d_r of the model with Ball–Berry stomatal conductance submodel (BB) was 0.879 for net photosynthesis rate (A_n) and 0.804 for stomatal conductance (g_s). d_r of the other model with Medlyn submodel (MED) was 0.881 for net photosynthesis rate (A_n) and 0.820 for stomatal conductance (g_s). NSE of the BB model was 0.941 for A_n and 0.798 for g_s. NSE of the MED model was 0.937 for A_n and 0.796 for g_s.

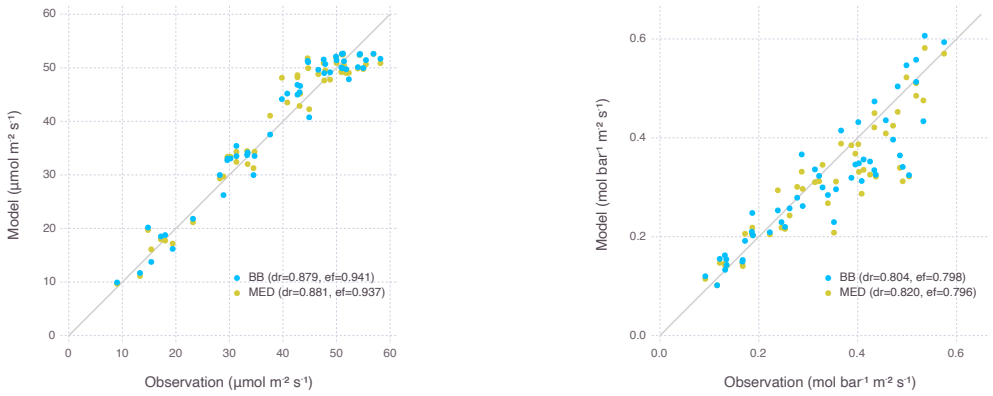

(**a**) Net photosynthesis rate (A_n) (**b**) Stomatal conductance (g_s)

Figure 1. Evaluation of the gas-exchange model with two stomatal conductance submodels, Ball–Berry (BB) and Medlyn (MED), after calibrating parameters related to nitrogen (N_0, s) and stomata (g_0, g_1). Each dot represents an observed photosynthesis rate (A_n) or stomatal conductance (g_s) under a given experimental condition and a corresponding estimation by the model. A gray solid line shows 1:1 reference for comparison. `dr` indicates Willmott's refined index of agreement (d_r), and `ef` indicates Nash–Sutcliffe modeling efficiency coefficient (NSE).

d_r values were close to 1, meaning our models were calibrated adequately for further analysis carried in the following sections, especially when it was achieved by calibrating only four parameters, while most other parameters came from existing models or literature (Table A2). The two variants of the gas-exchange model with different selection of the stomatal conductance submodel did not show a clear difference in their performance within the range of input given by our experimental dataset.

Although the difference between two gas-exchange models only came from how stomatal conductance was calculated in submodel, the pooled nature of our calibration process produced a slightly different set of parameters used by the other parts of model, such as nitrogen submodel shared between the two variants. For example, with baseline leaf nitrogen content (N_0) and steepness of nitrogen response curve (s) parameters, BB got 0.371 and 4.470, while MED got 0.315 and 3.912, respectively. To ensure their difference did not hamper comparison between two stomatal conductance models, we did a further sensitivity analysis on the two other parameters in Appendix C and confirmed the difference was negligible in regards with A_n response (Figure A7).

2.2. Stomatal Conductance Model Comparison

g_s predicted by MED was generally higher than g_s from BB (Figure 2). g_s from both models were in a similar range when relative humidity (RH) was around 65 % to 90 %, while maximum g_s was much higher in MED when RH was saturated. When RH went lower than 50 %, gs from BB dropped rapidly and mostly converged to the lower bound ($g_{0_{\mathrm{BB}}}$), almost shutting down transpiration. In MED, decrease of g_s along RH gradient was more gradual, and its value usually remained higher than the lower bound ($g_{0_{\mathrm{MED}}}$) to ensure a certain amount of transpiration keeps occurring.

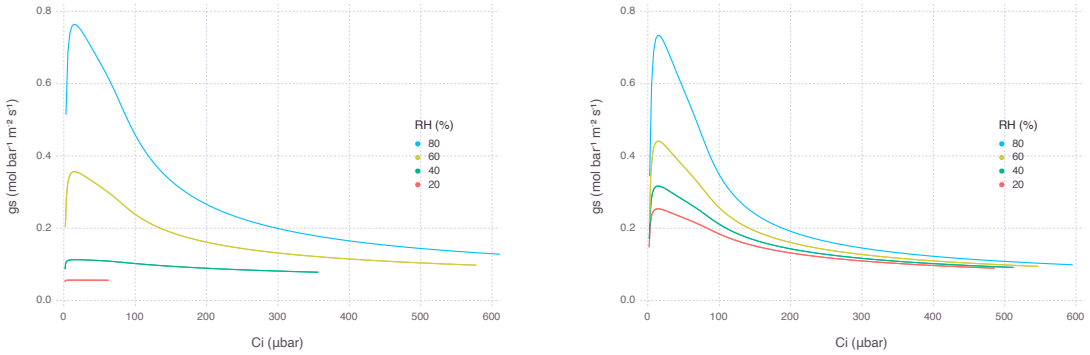

(**a**) Ball–Berry model (BB) (**b**) Medlyn model (MED)

Figure 2. Stomatal conductance (g_s) estimated by two stomatal conductance models over a range of atmospheric CO_2 concentration (C_a) from 10 µbar to 1500 µbar at multiple levels of relative humidity (RH). The graph was plotted against resultant intercellular CO_2 concentration (C_i). Air temperature (T_a) was 32 °C and irradiance (I) was 2000 $\mu mol_{quanta}\ m^{-2}\ s^{-1}$.

As a result, A_n from the gas-exchange model using BB decreased more rapidly, while the counterpart using MED showed a much gentle response as RH went down at the same level of concentration of atmospheric CO_2 (C_a). The rate of decrease in A_n was 75 % with BB and 20 % with MED when RH was dropped from 80 % to 20 %. However, there was little difference in the curvature of A_n response between the two models in terms of intercellular CO_2 concentration (C_i), suggesting the difference was mostly due to a change in supply function of the curve (Figure 3).

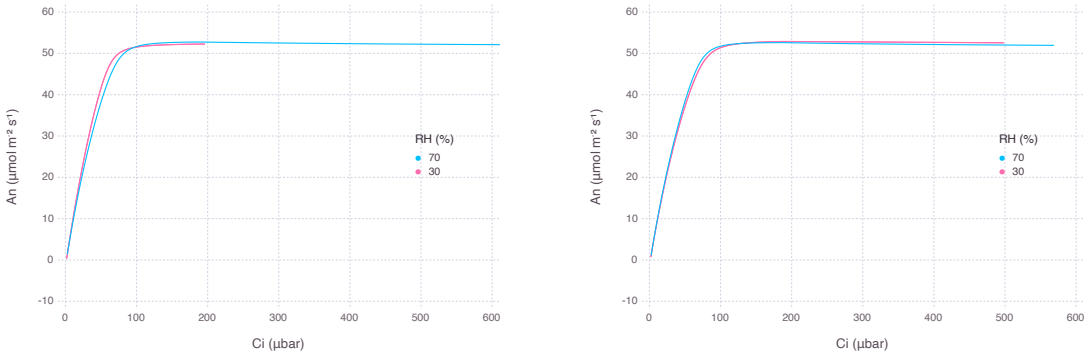

(**a**) Ball–Berry model (BB) (**b**) Medlyn model (MED)

Figure 3. Net photosynthesis rate (A_n) estimated by two stomatal conductance models over a range of atmospheric CO_2 concentration (C_a) from 10 µbar to 1500 µbar at two levels of relative humidity (RH). The graph was plotted against resultant intercellular CO_2 concentration (C_i). Air temperature (T_a) was 32 °C and irradiance (I) was 2000 $\mu mol_{quanta}\ m^{-2}\ s^{-1}$.

A similar response can be observed when A_n was plotted against a range of air temperature (T_a) from 0 °C to 50 °C (Figure 4). At lower RH, MED was able to maintain g_s to a certain level and therefore keep A_n from collapsing. The shifting of optimal temperature towards a higher regime with lower RH came from increased cooling effect by higher water loss in drier condition.

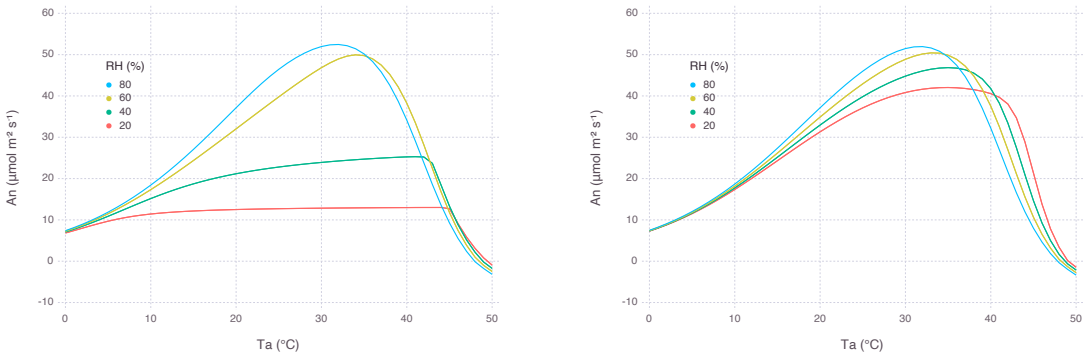

(**a**) Ball–Berry model (BB) (**b**) Medlyn model (MED)

Figure 4. Net photosynthesis rate (A_n) estimated by two stomatal conductance models over a range of air temperature (T_a) from 0 °C to 50 °C at multiple levels of relative humidity (RH). Atmospheric CO_2 concentration (C_a) was 400 µbar and irradiance (I) was 2000 $\mu mol_{quanta}\ m^{-2}\ s^{-1}$.

In turn, leaf temperature (T_l), which is adjusted by energy balance equation involving latent heat flux mainly driven by leaf transpiration, showed a clear difference between the two models. With BB, lower RH had stomata almost closed down and thus not able to cool down leaf temperature with latent cooling. On the contrary, MED implied higher latent cooling under lower RH due to stronger gradient of water vapor pressure formed between air and inside the leaf.

2.3. Stress Responses

2.3.1. Leaf Nitrogen Deficiency

A_n generally decreased as leaf nitrogen content (N) reduced and the rate of decrease accelerated when nitrogen was more limited as represented by logarithmic curves. Yet, the strength of response was not constant and varied depending on environmental conditions. A_n was more decreased with lower RH, but the difference diminished when N went below 0.5 $g\ m^{-2}$ or relative leaf nitrogen content (N_p) was less than 1 % assuming specific leaf area (SLA) was 200 $cm^2\ g^{-1}$. The rate of A_n decrease did not change much with high atmospheric CO_2 (C_a) and only had more negative effect when C_a was below 400 µmol mol^{-1}. Response to T_a under nitrogen stress was nonlinear that the decrease was more significant when T_a was moving away from optimal temperature. The optimal temperature, where a peak A_n could be achieved, slightly increased with more N available; thus, the maximum A_n itself also increased due to more favorable biochemical reactions with higher temperature and N (Figure 5c,g). The slope of A_n decrease by N stress was steeper under higher irradiance (I) and the difference between the levels of I gradually diminished as N approaching a minimum (Figure 5a,e). Overall, there was no clear difference in terms of nitrogen response between BB and MED models.

Ball–Berry (BB)

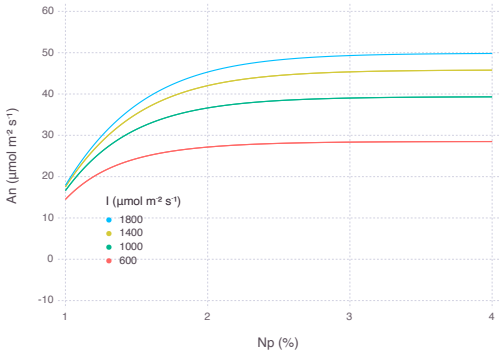

(**a**) Irradiance (I)

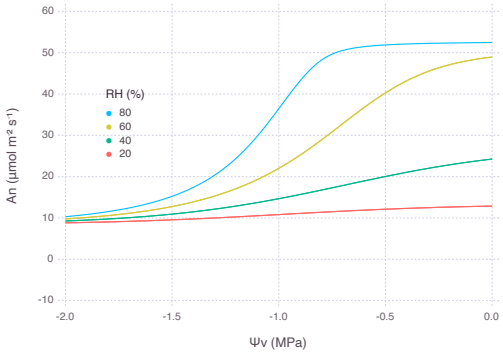

(**b**) Relative humidity (RH)

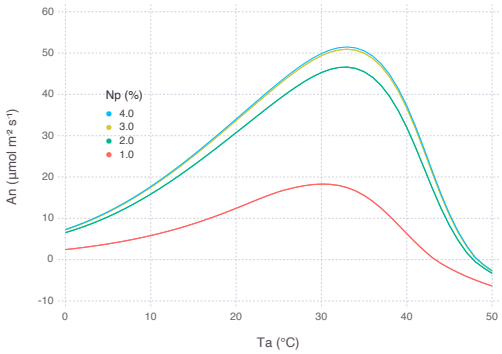

(**c**) Air temperature (T_a)

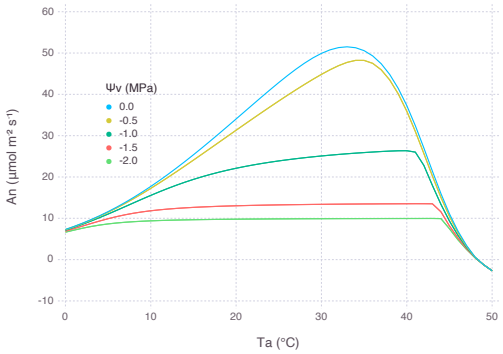

(**d**) Air temperature (T_a)

Medlyn (MED)

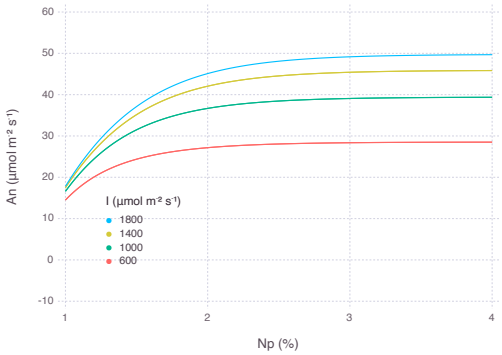

(**e**) Irradiance (I)

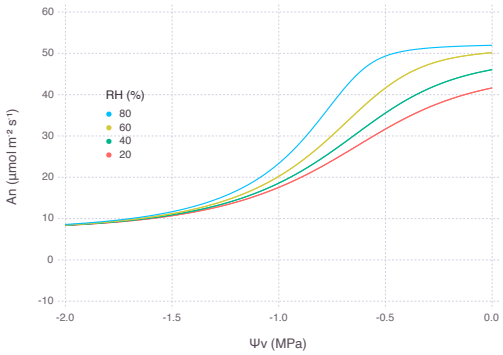

(**f**) Relative humidity (RH)

Figure 5. *Cont.*

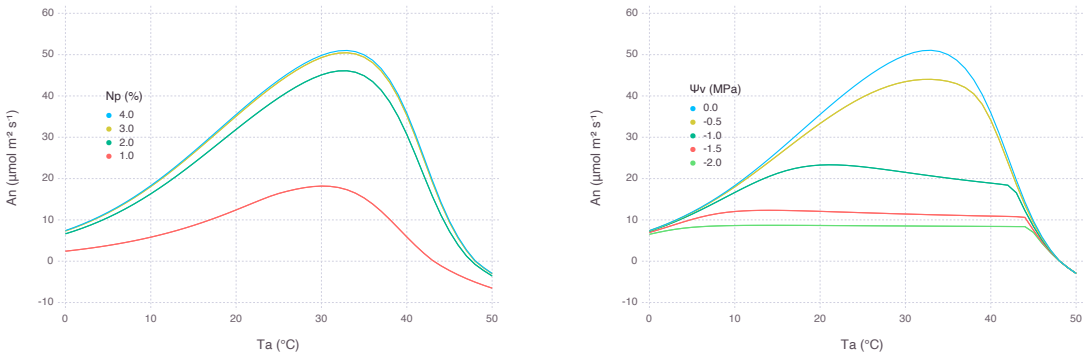

(**g**) Air temperature (T_a) (**h**) Air temperature (T_a)

Figure 5. Net photosynthesis rate (A_n) over a range of environmental input variables at multiple levels of nitrogen or water stress for the two variants of coupled gas-exchange model using Ball–Berry (BB) and Medlyn (MED) stomatal conductance submodels. (**a**,**c**,**e**,**g**) Responses to a varying degree of relative leaf nitrogen content (N_p) assuming specific leaf area (SLA) was 200 $cm^2\ g^{-1}$. (**b**,**d**,**f**,**h**) Responses to bulk leaf water potential (Ψ_v).

2.3.2. Leaf Water Status

A_n decreased as bulk leaf water potential (Ψ_v) reduced, but the rate of decrease did not monotonically change as in the case of nitrogen stress. Generally under a greater water stress with lower water potential, stress response represented by A_n reduction tapered off and formed a logistic response curve. A_n was more decreased with lower RH, but the difference diminished when Ψ_v kept decreasing. In addition, note that with higher RH, leaf was able to sustain maximum A_n even under mild water deficit which would have led to a noticeable reduction in A_n under lower RH. For example, at −0.4 MPa, A_n under 80 % of RH did not decrease much, whereas A_n under 40 % of RH saw almost 60 % reduction with BB (Figure 5b) and 20 % reduction with MED (Figure 5f). The decrease of A_n was more consistent with all range of C_a compared to nitrogen stress response. For −1.5 MPa and below, the rate of A_n decrease became almost identical regardless of C_a. With higher C_a, maximum A_n was sustained for larger range of Ψ_v similar to the RH response. Water response to T_a was also nonlinear, but the difference wore off with lower Ψ_v and no single optimal temperature was clear to be found (Figure 5d,h). Overall response to T_a under water stress was similar between BB and MED, except BB exhibited much higher optimal temperature than MED in a mild-to-severe stress level, indicated by −1.0 MPa. Overall, BB was more sensitive to RH changes under water stressed conditions than MED (Figure 5d,f).

2.4. Interactions between Leaf Nitrogen and Water Potential

2.4.1. Response to Relative Humidity

At high RH, A_n remained relatively stable within its optimal range when both N and Ψ_v kept high for less stress (Figure 6a,g). An area of this region located in the upper right side of contour plot shrunk and so did the range of non-limiting N and Ψ_v as RH went down. In other words, with lower RH, A_n became more sensitive to both nitrogen and water stress factors. The reduction of A_n for lower RH was extremely strong with BB (Figure 6d) compared to MED (Figure 6j). No other variables showed such drastic difference between BB and MED in the comparison.

Note that, with low N and high Ψ_v, the sensitivity of A_n was mostly governed by the change of N, thus limited by nitrogen. On the other hand, with high N and low Ψ_v, the most of sensitivity came from the change of Ψ_v, thus limited by water. Then, with both low N and Ψ_v, A_n was also largely driven by Ψ_v unless N dropped down to a very low range.

2.4.2. Response to Atmospheric CO_2

The upper-right region of non-limiting A_n existed with a range of C_a above 400 µbar. This region vertically expands further down to cover lower Ψ_v under higher C_a, as shown by comparing ambient CO_2 (Figure 6e,k) with elevated CO_2 (Figure 6b,h), indicating possible alleviation of water stress by elevated CO_2 concentration. A_n remained relatively stable until Ψ_v reached down to −1.0 MPa under 800 µbar of C_a, whereas A_n started decreasing faster only after −0.5 MPa under 400 µbar of C_a. Below these boundaries, A_n was mostly limited by water only.

2.4.3. Response to Irradiance

The region of non-limiting A_n remained relatively stable with a range of I (Figure 6c,i) and even expanded further down when I was lower, although the magnitude of A_n was much smaller (Figure 6f,l). In other words, under shaded condition with less light, nitrogen and water became less relevant because A_n had to be much smaller. Below this region, A_n was again mostly limited by water only unless N deficiency was extremely strong.

Ball–Berry (BB)

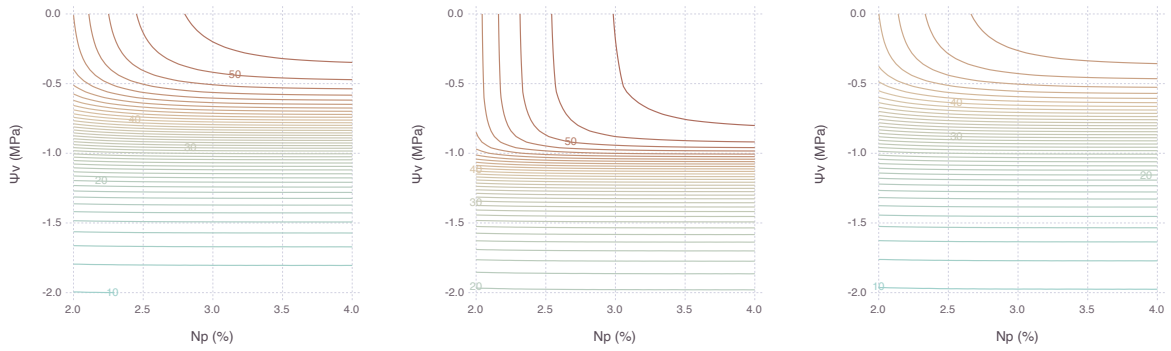

(**a**) RH = 70 % (**b**) C_a = 800 µbar (**c**) I = 1500 µmol m^{-2} s^{-1}

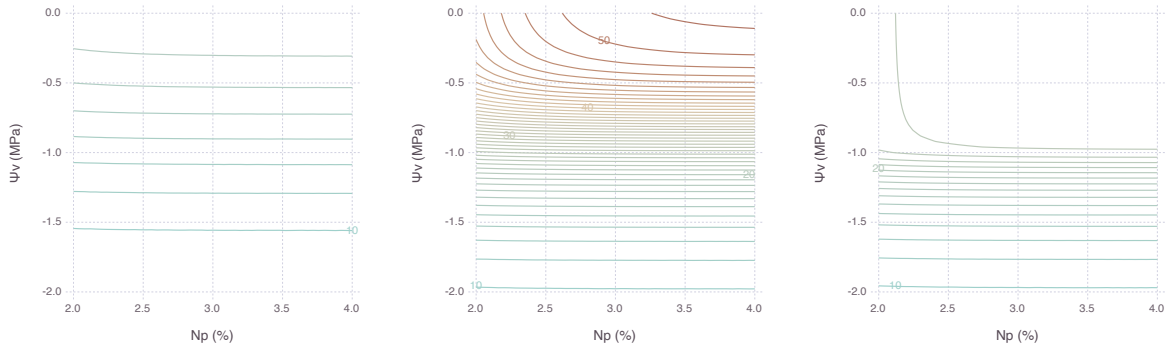

(**d**) RH = 30 % (**e**) C_a = 400 µbar (**f**) I = 500 µmol m^{-2} s^{-1}

Figure 6. *Cont.*

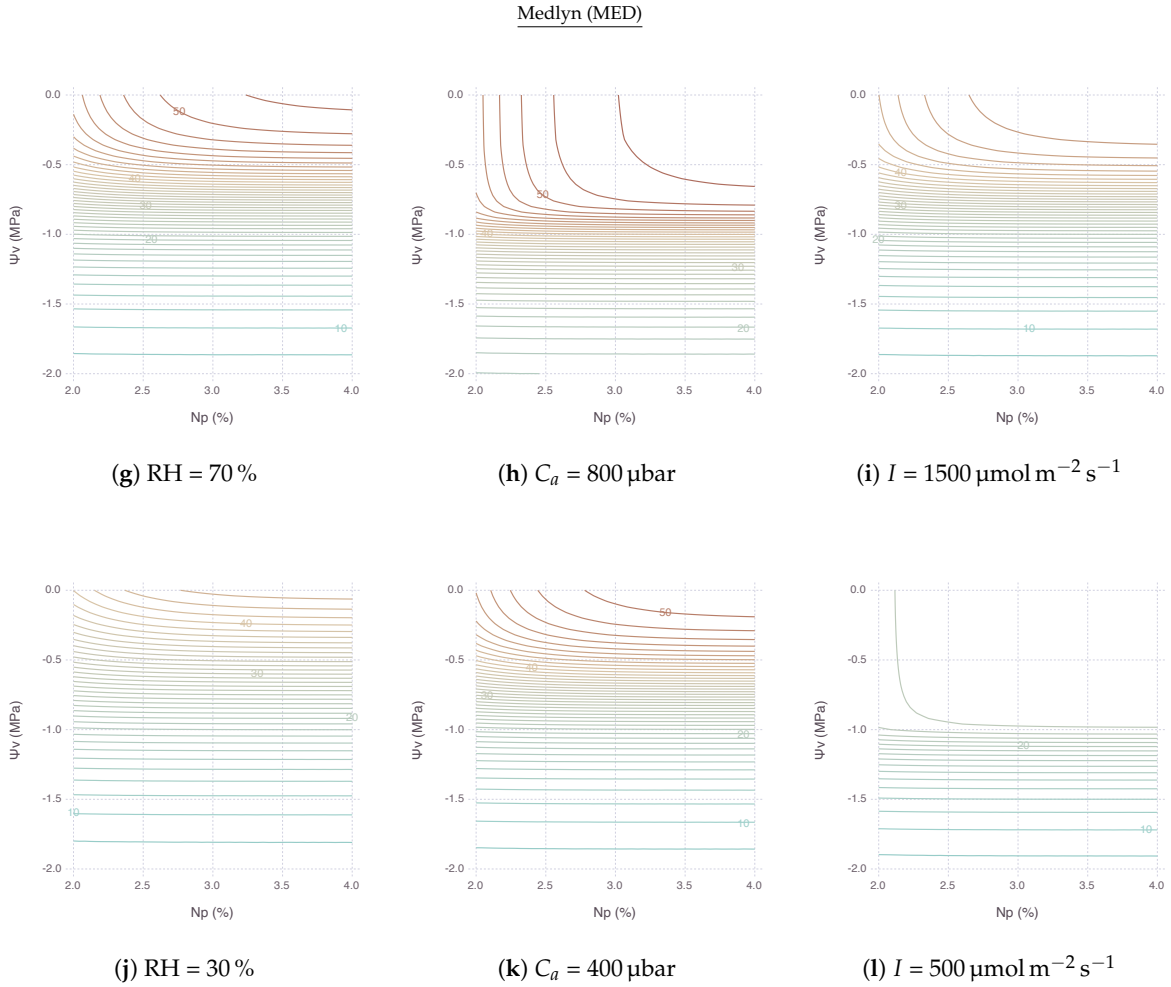

(**g**) RH = 70 % (**h**) C_a = 800 µbar (**i**) I = 1500 µmol m^{-2} s^{-1}

(**j**) RH = 30 % (**k**) C_a = 400 µbar (**l**) I = 500 µmol m^{-2} s^{-1}

Figure 6. Responses of net photosynthesis rate (A_n) under nitrogen and water stress implied by relative leaf nitrogen content (N_p) and bulk leaf water potential (Ψ_v) for the two variants of coupled gas-exchange model using Ball–Berry (BB) and Medlyn (MED). (**a**,**d**,**g**,**j**) Contrasting effects of high and low relative humidity. (**b**,**e**,**h**,**k**) Comparison between elevated and current concentrations of atmospheric CO_2 (C_a). (**c**,**f**,**i**,**l**) Comparison between high and low levels of irradiance (I). Contour lines are spaced at an interval of 1 µmol m^{-2} s^{-1} of the simulated A_n values.

3. Discussion

3.1. Performance of Stomatal Conductance Models

We did not find much difference in performance between two stomatal conductance submodels BB and MED when used for fitting calibration dataset (Figure 1). It is known that two models have equal predictive strength for non-extreme environmental conditions where the data are usually collected for calibration and validation [25]. Results started deviating from each other under more extreme conditions, such as low C_a and low RH, which are also close to the range where gas-exchange instruments often find difficulties in accurate measurements (Figures 2–5b,f). Under low RH, especially below 50 %, $g_{s_{BB}}$ had much higher rate of decrease and almost converged to $g_{0_{BB}}$ in the end, whereas $g_{s_{MED}}$ maintained higher than $g_{0_{MED}}$ with smooth and gentle transitions most of the time (Figure 2). Seemingly degenerate behavior of $g_{s_{BB}}$ might be an overlooked effect of $g_{0_{BB}}$ as a parameter estimated from regression rather than a directly measured value [26]. A clearly different response from each model warrants caution, especially when applying models to extreme conditions, such as concurrent exposure to high temperature and high vapor pressure deficit (VPD), likely encountered in future climate projections [27].

3.2. Stress Response to Elevated CO_2

Nitrogen stress consistently posed a negative impact on A_n although the degree of reduction may vary depending on the severity of stress and corresponding environmental conditions (Figure 5a,c,e,g). While water stress also reduced A_n in most of the time (Figure 5b,d,f,h), we observed in some conditions that the impact of water stress greatly diminished, for instance, when RH was higher than 60 % (Figure 6a,g) or C_a was higher than 400 µmol mol^{-1} (Figure 6b,h). There is increasing evidence that elevated CO_2 concentration alleviates water stress [28–34]. Our simulation result confirms this positive effect of elevated CO_2 by showing high A_n sustained in a wider range of Ψ_v under high C_a due to reduced g_s preserving water loss via transpiration. The effect was mostly pronounced under a mild water stressed condition since maximum A_n did not change much in the absence of water stress [35]. Alleviation strength was dependent on leaf nitrogen supply such that even very mild water stress could not be overcome by high C_a under low N [33].

3.3. Interactions between Nitrogen Deficiency and Water Stress

When both nitrogen and water stress were imposed simultaneously, the net effect of stress may vary depending on the relative degree of each stress factor and environmental variables. In the contour plots of interactive stress effects, we can identity three types of contours (Figure 5). Mostly vertical lines with very steep slopes indicate A_n could be only improved by moving across a horizontal gradient, conferring a dominant N sensitivity. Likewise, mostly horizontal lines with a slope close to zero indicate A_n could be only improved by moving across a vertical gradient, conferring a dominant Ψ_v sensitivity. Other curves from round contour lines indicate A_n are affected by both stress factors. With that in mind, looking back stress interaction result figures gives an insight that a vast area of N and Ψ_v grid are covered by horizontal lines; thus, they are mostly under water limiting conditions. Nitrogen limiting conditions are, on the other hand, exhibited within an area where N is low or Ψ_v is high. Such distinctions could be also found in literature where the negative impact of nitrogen stress could be inflated by an existence of drought stress [30,36–38].

3.4. Response of Transgenic C_4 Leaves to Temperature

As an extended exercise for testing model response against real conditions, we applied our model to simulate a wide range of temperature response of transgenic C_4 plants, *Flaveria bidentis*, with varying amount of Rubisco reported by Kubien et al. [39]. By using a set of slightly modified parameters, as described in Appendix D, we were able to replicate overall patterns of A_n (Figure 7d) and C_i (Figure 7f) over a wide range of T_l using MED. The performance of BB was close to MED, except that C_i, under low T_a with more reduced Rubisco (AR2), showed an abrupt change due to g_s that went too low, reaching the lower bound $g_{0_{BB}}$ (Figure 7a,c).

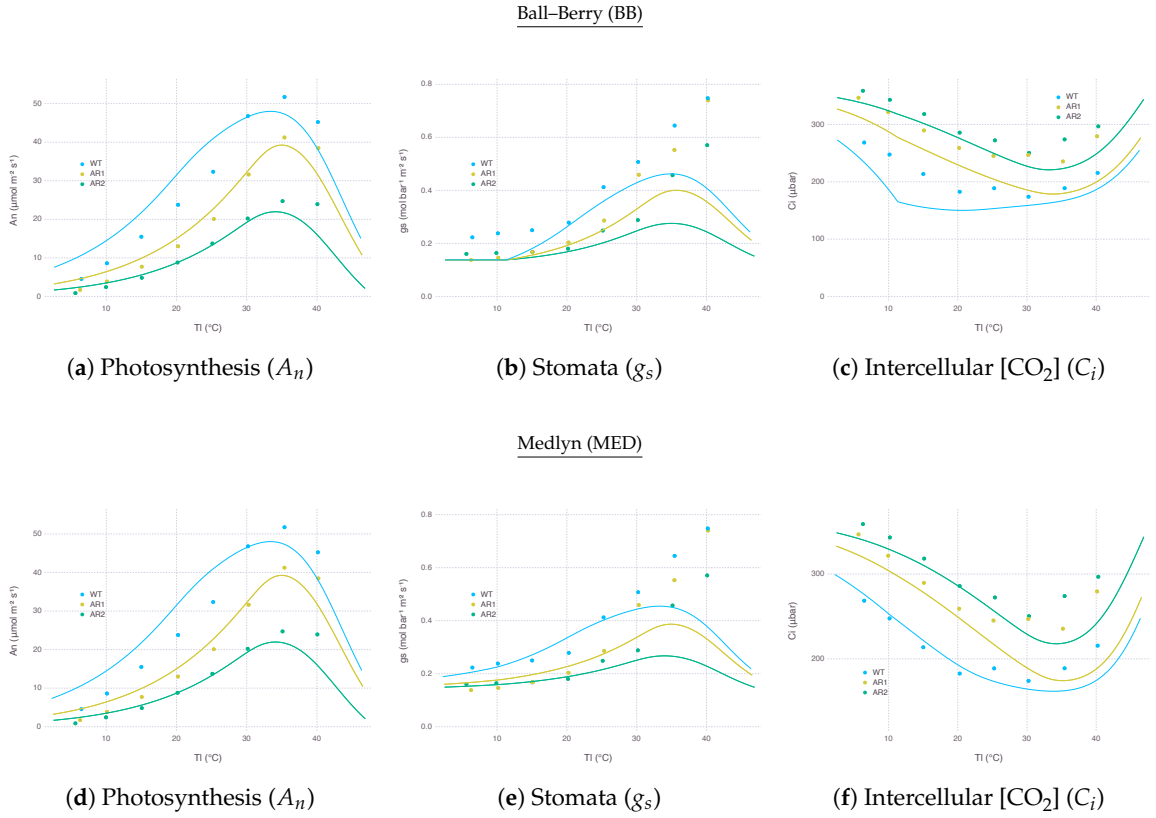

(**a**) Photosynthesis (A_n) (**b**) Stomata (g_s) (**c**) Intercellular [CO_2] (C_i)

(**d**) Photosynthesis (A_n) (**e**) Stomata (g_s) (**f**) Intercellular [CO_2] (C_i)

Figure 7. Gas-exchange simulation results over a range of leaf temperature for wild type (WT) and mutants (AR1, AR2) *Flaveria bidentis* leaves with Rubisco content reduced to 49 % and 32 %, respectively, to replicate Figure 1 of Kubien et al. [39]. Variables and parameters modified for this simulation are listed in Table A3. Other parameters remained the same as listed in Table A2. Solid curves represent model estimation for each treatment. Dots indicate data points digitized from the result of original experiment.

Simulated g_s closely followed the actual measurements until around 35 °C where model and observation started showing disagreement (Figure 7b,e). In the experiment, g_s kept increasing further with higher T_l, whereas our model estimated g_s should decrease when A_n was not able to keep up under excessive heat stress. Such decreasing patterns occurred regardless of stomatal conductance submodels. This behavior is indeed contrary to observations where transpiration rate continually increases with higher leaf temperature, implying A_n inhibition is not caused by stomatal closure; thus, A_n should decouple from g_s for some species [40,41]. However, this mechanism is not easily applicable to many if not all commonly used gas-exchange models relying on empirical relationship between A_n and g_s, as explained in Appendix A.5. Alternative stomatal conductance models with mechanistic understandings on stomata responses to humidity and temperature could be useful for simulating field conditions where temperature fluctuates more than humidity [42,43]. In the meantime, more attention should be paid to the current results of gas-exchange models under high temperature, which is especially critical when simulating climate change scenarios.

4. Materials and Methods

4.1. Model Structure

The gas-exchange model consists of a number of smaller submodels describing different aspect of biochemical and physical processes coupled to each other following the structure of Kim and Lieth [7]. The C_4 photosynthesis is coupled with a stomatal conductance model via net photosynthesis rate (A_n) and also interacts with energy balance model to establish leaf temperature (T_l) [44]. We tested two

stomatal conductance models, Ball–Berry model (BB) and Medlyn model (MED), combined with the rest of submodels remained the same, yielding two variations of the gas-exchange model. More details about the model specification are given in Appendix A.

4.2. Model Calibration

Most of parameter values came from existing literatures (Table A2). Some photosynthetic parameters were obtained from Pioneer hybrid 3733 maize (*Zea mays*) grown under Soil–Plant–Atmosphere Research (SPAR) chambers located at Beltsville, MD, USA, in 2002 [45]. Only four parameters were specifically calibrated for modeling experiments presented in this paper. Two are nitrogen-related parameters: baseline leaf nitrogen content (N_0) and steepness of nitrogen response curve (s). The other two are related to stomatal conductance: lower bound of stomatal conductance (g_0) and sensitivity of stomatal conductance (g_1). For comparison of overall gas-exchange response between two stomatal conductance models, calibration was separately done for the two models: Ball–Berry (BB) and Medlyn (MED) models.

N_0 and s calibrated for BB and MED were then pooled together to provide average parameter values used by the both models. To make sure a slight divergence in the parameter value did not make an impact on overall model response, we also conducted a sensitivity analysis on N_0 and s for a range of possible values. As g_0 and g_1 should involve inherent differences between two stomatal conductance models, a separate set of parameter values were used accordingly. BB model relied on $g_{0_{\mathrm{BB}}}$ and $g_{1_{\mathrm{BB}}}$. MED model relied on $g_{0_{\mathrm{MED}}}$ and $g_{1_{\mathrm{MED}}}$. The optimization method used for calibration was differential evolution algorithm [46].

The experimental dataset for calibration was collected from a growth chamber experiment conducted with Pioneer hybrid 34N43 maize in 2005 at Beltsville, MD, USA, as used in Kim et al. [44,47]. Spot measurements of gas-exchange were recorded with LI-COR LI-6400XT when plants were at the onset of reproductive stage. Three nitrogen levels at 0 kg ha^{-1}, 50 kg ha^{-1} and 200 kg ha^{-1} in total were applied two times. For leaf nitrogen content (N), SPAD measurements were instead collected with Konica Minolta SPAD-502 and converted to N, as described in Appendix B.

The fitness of model calibration was evaluated by Willmott's refined index of agreement d_r as defined in Equation (1) [48] and Nash–Sutcliffe modeling efficiency coefficient (NSE) as defined in Equation (2) [49]. y_i is an observed value for the variable of interest under a specific environmental condition ordered by i. $\hat{y}_i$ is an estimation by the model for the same input condition as y_i. $\bar{y}$ is the mean of observed values. Net photosynthetic rate (A_n) and stomatal conductance (g_s) were two variables selected for the evaluation.

$$
\begin{aligned}
a &= \sum_i |\hat{y}_i - y_i| \\
b &= 2\sum_i |y_i - \bar{y}| \\
d_r &= \begin{cases} 1 - \frac{a}{b} & \text{if } a \le b \\ \frac{b}{a} - 1 & \text{otherwise} \end{cases}
\end{aligned} \tag{1}
$$

$$
NSE = 1 - \frac{\sum_i (\hat{y}_i - y_i)^2}{\sum_i (y_i - \bar{y})^2} \tag{2}
$$

4.3. Model Comparison

We compared two variants of the gas-exchange model depending on which submodel was used for calculating stomatal conductance: Ball–Berry (BB) and Medlyn (MED). Net photosynthetic rate (A_n) was calculated over a range of values for specific environmental input variables, atmospheric CO_2 and air temperature (T_a). C_a ranged from 0 µbar to 1500 µbar and T_a ranged from −10 °C to

50 °C. Other environmental variables remained constant as default values (Table 1). Since stomatal conductance can be more directly related to the relative humidity of surrounding air (RH) than other variables, a response curve of A_n was separately obtained for ten levels of RH from 0 % to 100 %.

Table 1. Default values for environmental input variables.

Symbol	Value	Units	Description
C_a	400	µbar	Atmospheric CO_2 partial pressure
P_a	99.4	kPa	Atmospheric pressure
T_a	32	°C	Air temperature in Celsius
I	2000	$\mu mol_{quanta}\, m^{-2}\, s^{-1}$	Incident PAR
u	2	$m\, s^{-1}$	Wind speed
RH	66	%	Relative humidity of the air
SPAD	60	-	SPAD value

4.4. Model Response

We simulated nitrogen and water stress factors by adjusting relevant parameter values. For nitrogen stress, leaf nitrogen content (N) was changed from 0 $g\, m^{-2}$ to 2 $g\, m^{-2}$ to impose stress when N was lower. For water stress, bulk leaf water potential (Ψ_v) was changed from 0 MPa down to −3 MPa to impose stress when Ψ_v was lower. The range of values were deliberately chosen by first selecting biophysically feasible extremes, 0 $g\, m^{-2}$ for N and 0 MPa for Ψ_v, then selecting a value for the other end where output variable exhibits a clear convergence. When simulating a response for each stress factor, the other stress factor assumed to be not limiting. The response curve of net photosynthetic rate (A_n) was obtained for multiple environmental input variables including relative humidity (RH), atmospheric CO_2 (C_a), air temperature (T_a), and irradiance (I).

In order to observe interaction effects between the two stress factors, contour plot of A_n was obtained by applying the same range of two stress factors simultaneously. For each environmental input variable, four different levels of the value were chosen to show a varying contrast as the input changes. RH changed to 30, 50, 70 and 90 %. C_a changed to 200, 400, 600 and 800 µbar. I changed to 500, 1000, 1500 and 2000 $\mu mol\, m^{-2}\, s^{-1}$.

5. Conclusions

We compared how two stomatal conductance models, Ball-Berry (BB) and Medlyn (MED), perform when coupled with the C_4 photosynthesis model of von Caemmerer [12]. Traditionally, BB has been widely used in leaf gas-exchange modeling research. More recently proposed MED approach is founded upon BB approach to provide physiological underpinnings of empirical parameters and has been considered as an alternative to BB. Our results confirmed that the performance of two models were comparable in a wide range of environmental conditions, yet could deviate substantially in low humidity conditions.

We further tested applicability of the model by replicating the behavior of transgenic C_4 leaves under moderate temperatures found in the literature. The coupled model, however, underestimated stomatal conductance in very high temperatures, presumably due to an inherent limitation of the coupling approaches using Ball–Berry type models in which photosynthesis and stomatal conductance are recursively linked as an input of the other.

We were able to reach these findings thanks to a novel modeling framework written in Julia programming language used for model development and analysis [50]. Our modeling approach is extensible and can be a useful means for studying the ecophysiology of C_4 plants, including staple and energy crops, such as maize, sorghum, and switchgrass.

Author Contributions: Conceptualization, S.-H.K.; methodology, K.Y., D.T., S.-H.K.; software, K.Y.; validation, K.Y., S.-H.K.; formal analysis, K.Y., S.-H.K.; investigation, K.Y., S.-H.K.; resources, D.T., S.-H.K.; data curation, K.Y., S.-H.K.; writing–original draft preparation, K.Y.; writing–review and editing, K.Y., D.T., S.-H.K.; visualization, K.Y.; supervision, S.-H.K.; project administration, S.-H.K.; funding acquisition, S.-H.K. All authors have read and

agreed to the published version of the manuscript. All authors have read and agreed to the published version of the manuscript.

Funding: The information, data, or work presented herein was funded in part by the Advanced Research Projects Agency-Energy (ARPA-E), U.S. Dept of Energy, under Award Number DE-AR0000820; by the Cooperative Agreement between the Agricultural Research Service, U.S. Dept of Agriculture and University of Washington under Agreement Number 58-8042-6-097; and by the Cooperative Research Program for Agricultural Science and Technology Development, Rural Development Administration, Republic of Korea under Grant Number PJ015124012020. The views and opinions of authors expressed herein do not necessarily state or reflect those of the United States Government, the Korean Government, or any agency thereof.

Conflicts of Interest: The authors declare no conflict of interest.

Abbreviations

The following abbreviations are used in this manuscript:

BB	Ball–Berry stomatal conductance model [10]
CAM	Crassulacean Acid Metabolism
FvCB	Farquhar–von Caemmerer–Berry model [9]
MED	Medlyn stomatal conductance model [11]
NSE	Nash–Sutcliffe model efficiency coefficient [49]
PAR	Photosynthetic Active Radiation
PEPC	Phosphoenolpyruvate Carboxylase
PPFD	Photosynthetic Photon Flux Density
PRMSE	Percentage Root Mean Square Error
PSII	Photosystem II
RH	Relative Humidity
SLA	Specific Leaf Area
SPAD	Soil Plant Analysis Development
SPAR	Soil–Plant–Atmosphere Research
VPD	Vapor Pressure Deficit
WT	Wild type
AR1, AR2	Mutants with reduced Rubisco content

Appendix A. Gas-Exchange Model Specification

Appendix A.1. C_4 Photosynthesis

The biochemical demand for CO_2 assimilation in C_4 leaves was adapted from an existing C_4 photosynthesis model [12]. The rate of net CO_2 assimilation (A_n) was represented by the minimum of enzyme limited (A_c) and electron transport limited (A_j) CO_2 assimilation rates with curvature factor β.

$$A_n = \min h\{A_c, A_j, \beta\} \tag{A1}$$

The transition between A_c and A_j was calculated using a hyperbolic minimum where $\min h\{a, b, c\}$ is equivalent to taking the lower root of quadratic equation $cx^2 - (a + b)x + ab = 0$ with curvature factor c interpreted as a parameter of co-limitation [51,52]. A_c can be approximated by the minimum of phosphoenolpyruvate carboxylase (PEPC) activity (A_{c_1}) and Rubisco activity (A_{c_2}) taking into account the bundle-sheath leakage and mitochondrial respiration. A_c is driven by A_{c1} under low [CO_2] and by A_{c2} under high [CO_2].

$$A_c = \min\{A_{c_1}, A_{c_2}\} \tag{A2}$$

$$A_{c_1} = V_p + g_{bs}C_m - R_m \tag{A3}$$

$$A_{c_2} = V_{c\max} - R_d \tag{A4}$$

V_p is the rate of C_4 carboxylation and assumed to be limited either by PEPC activity or PEP regeneration. g_{bs} is the bundle sheath conductance to CO_2 and C_m is the mesophyll CO_2 partial pressure.

V_{cmax} is the maximum rate of Rubisco carboxylation (μmol $\mathrm{m}^{-2}\,\mathrm{s}^{-1}$). R_d is mitochondrial respiration in the light (μmol$_{\mathrm{CO_2}}$ $\mathrm{m}^{-2}\,\mathrm{s}^{-1}$) and half of its value was assumed a mesophyll component, R_m.

$$V_p = \min\left\{\frac{C_m V_{p\mathrm{max}}}{C_m + K_p}, V_{pr}\right\} \tag{A5}$$

$V_{p\mathrm{max}}$ is the maximum PEP carboxylation rate, K_p is the Michaelis-Menton constant for CO_2 of PEPC, and V_{pr} is PEP regeneration rate. Provided that the resistance for CO_2 from intercellular spaces to mesophyll cells is negligible, C_m can be estimated from CO_2 partial pressure of the air (C_a) after taking account of total leaf resistance to CO_2 (r_{v_c}) under a given A_n.

$$C_m \approx C_i = C_a - A_n r_{v_c} \tag{A6}$$

$$r_{v_c} = r_{s_c} + r_{b_c} \tag{A7}$$

$$r_{s_c} = \frac{1}{g_s} \cdot \left(\frac{\mathcal{D}_w}{\mathcal{D}_c}\right)^1 \tag{A8}$$

$$r_{b_c} = \frac{1}{g_b} \cdot \left(\frac{\mathcal{D}_w}{\mathcal{D}_c}\right)^{\frac{2}{3}} \tag{A9}$$

The ratio between diffusion coefficient for water vapor ($\mathcal{D}_w$) and CO_2 ($\mathcal{D}_c$) is used for converting from stomatal conductance (g_s) and boundary layer conductance (g_b) in terms of CO_2 into resistance in terms of water vapor (r_{s_c}, r_{b_c}). We assume g_s is subject to still air and thus raised to the power of 1, whereas g_b is subject to convective air with laminar flow and thus raised to the power of $\frac{2}{3}$ [53,54].

C_m was solved numerically by using bisection method because its dependence on A_n which is required in the calculation of g_s forms a cyclic dependency difficult to be solved analytically.

The assimilation rate limited by electron transport (A_j) can be approximated similarly to A_c by the minimum of electron transport limited rates in C_4 and C_3 cycles.

$$A_j = \min\{A_{j_1}, A_{j_2}\} \tag{A10}$$

$$A_{j_1} = \frac{xJ}{2} - R_m + g_{bs} C_m \tag{A11}$$

$$A_{j_2} = \frac{(1-x)J}{3} - R_d \tag{A12}$$

Total rate of electron transport (J) was modeled using a non-rectangular hyperbola which can be described with hyperbolic minimum (min$h$). x is a partitioning factor of J.

$$J = \min h\{I_2, J_{\mathrm{max}}, \theta\} \tag{A13}$$

θ is curvature of response of electron transport to photosynthetically active radiation (PAR) and J_{max} is the maximum rate of electron transport. I_2 is effective radiation absorbed by Photosystem II (PSII) [7,55].

$$I_2 = \frac{(1-f)}{2} I_a \tag{A14}$$

$$I_a = \alpha I \tag{A15}$$

I is the incident light in photosynthetic photon flux density (PPFD) and I_a is PPFD absorbed by the leaf. α is leaf absorptance in PAR and assumed $1 - \delta$ where δ is the proportion of the incident light scattered by the leaf surface. f is the spectral correction factor. PAR assumes the wave band of solar radiation from 400 nm to 700 nm.

The temperature dependence of $V_{p\max}$, $V_{c\max}$, and R_d was approximated by the Arrhenius equation (k_{T_A}) normalized at a base temperature.

$$k_{T_A}[T_k, E_a] = \exp\left[\frac{E_a(T_k - T_{b_k})}{R \cdot T_k \cdot T_{b_k}}\right] \tag{A16}$$

E_a is the activation energy varies by process, T_l is the leaf temperature and T_b is the base temperature assumed 25 °C. T_{l_k} and T_{b_k} are corresponding absolute temperatures in Kelvin (K). R is the universal gas constant. Each temperature dependent parameter has a value at 25 °C.

The temperature dependence of K_p and V_{pr} was assumed to be Q_{10} of 2.0.

$$k_{T_Q}[T] = Q_{10}^{\frac{T-T_b}{10}} \tag{A17}$$

The temperature dependence of $J_{\max}$ was modeled using a peaked function [56].

$$k_{T_P}[T_k, E_a, H, S] = k_{T_A}[T_k, E_a] \cdot \left(1 + \exp\left[\frac{S \cdot T_{b_k} - H}{R \cdot T_{b_k}}\right]\right)\left(1 + \exp\left[\frac{S \cdot T_k - H}{R \cdot T_k}\right]\right)^{-1} \tag{A18}$$

E_a and R are as defined above. H is the curvature parameter determining the rate of decrease above the peak temperature and S is the entropy factor.

Nitrogen dependence of $V_{p\max}$, $V_{c\max}$, and $J_{\max}$ was modeled by a logistic function for the current leaf nitrogen content (N) [20]. N_0 is a baseline value assumed for the leaf nitrogen content and s is the steepness of nitrogen response curve.

$$k_N = \frac{2}{1 + \exp[-s \cdot \max\{N_0, N\} - N_0]} - 1 \tag{A19}$$

Temperature dependence (k_T) and nitrogen dependence (k_N) are multiplicative limiting factors. For example, electron transport rate ($V_{p\max}$) is scaled from $V_{p\max_{25}}$ by calculating $V_{p\max} = V_{p\max_{25}} \cdot k_{T_A}[T_l, E_{ap}] \cdot k_N$ with the current leaf temperature (T_l) and an activation energy for PEPC (E_{ap}).

Appendix A.2. Boundary Layer Conductance

Boundary layer conductance to water vapor (g_b) was derived from convective heat conductance of the leaf surface (g_H). Corresponding Nusselt number (Nu) and Reynolds Number (Re) were derived by assuming forced convection of streamline flow on flat plates [57]. u is wind speed (m s^{-1}) and d is characteristic dimension of the leaf determined by leaf width W (cm) [53]. $\mathcal{D}_m$ is kinematic viscosity of the air and $\mathcal{D}_h$ is thermal diffusivity of the air. $\mathcal{D}_m$ and $\mathcal{D}_h$ were assumed temperature independent at 20 °C.

$$g_H = \frac{\mathcal{D}_h \cdot \mathrm{Nu}}{d} \tag{A20}$$

$$\mathrm{Nu} = 0.60\sqrt{\mathrm{Re}} \tag{A21}$$

$$\mathrm{Re} = \frac{u \cdot d}{\mathcal{D}_m} \tag{A22}$$

$$d = 0.72w \tag{A23}$$

g_H (m s^{-1}) is then scaled and converted to g_h (mmol m^{-2} s^{-1}) using the Gas Laws [57]. T_{a_k} is the absolute temperature of air (K).

$$g_h = g_H \cdot \frac{P_a}{R \cdot T_{a_k}} \tag{A24}$$

g_b was then derived from g_h using a diffusion ratio between water vapor and heat transfer under forced convection [53,54]. Additionally, g_b was normalized to the current atmospheric pressure (P_a) to make its units explicitly expressed in vapor pressure gradient rather than in unitless mole fraction.

$$g_b = \frac{g_h}{P_a} \cdot \left(\frac{\mathcal{D}_w}{\mathcal{D}_h}\right)^{\frac{2}{3}} \tag{A25}$$

Appendix A.3. Stomatal Conductance

We used two approaches for modeling stomatal conductance (g_s). $g_{s_{\mathrm{BB}}}$ is stomatal conductance following Ball–Berry (BB) model [10] and $g_{s_{\mathrm{MED}}}$ follows Medlyn (MED) model [11].

$$g_{s_{\mathrm{BB}}} = g_{0_{\mathrm{BB}}} + g_{1_{\mathrm{BB}}} \frac{h_s A_n}{C_s} f_{\Psi_v} \tag{A26}$$

$g_{0_{\mathrm{BB}}}$ ($\mathrm{mol_{H_2O}\,m^{-2}\,s^{-1}\,bar^{-1}}$) is residual stomatal conductance to water vapor at the light compensation point and $g_{1_{\mathrm{BB}}}$ is the empirical coefficient for the sensitivity of g_s to other variables. h_s is relative humidity at the leaf surface (as a fraction), A_n is net photosynthesis, and P_a is the partial pressure of the air.

f_{Ψ_v} is a weight factor that adjusts stomatal conductance to the bulk leaf water potential (Ψ_v) where Ψ_f is a reference potential and s_f is a sensitivity parameter [8].

$$f_{\Psi_v} = \frac{1 + \exp\left[s_f \Psi_f\right]}{1 + \exp\left[s_f(\Psi_f - \Psi_v)\right]} \tag{A27}$$

$g_{s_{\mathrm{MED}}}$ has a slightly different form compared to $g_{s_{\mathrm{BB}}}$ that uses vapor pressure deficit at the leaf surface (D_s) instead of h_s. $g_{0_{\mathrm{MED}}}$ ($\mathrm{mol_{H_2O}\,m^{-2}\,s^{-1}\,bar^{-1}}$) has the same meaning as $g_{0_{\mathrm{BB}}}$ setting a lower bound of the conductance value. $g_{1_{\mathrm{MED}}}$ is similarly a sensitivity parameter, but in different units ($\sqrt{\mathrm{kPa}}$) and scale.

$$g_{s_{\mathrm{MED}}} = g_{0_{\mathrm{MED}}} + \left(1 + \frac{g_{1_{\mathrm{MED}}}}{\sqrt{D_s}}\right) \frac{A_n}{C_s} f_{\Psi_v} \tag{A28}$$

In both models, C_s is CO_2 partial pressure at the leaf surface after taking account of boundary layer resistance to CO_2 (r_{b_c}) under a given A_n.

$$C_s = C_a - A_n r_{b_c} \tag{A29}$$

h_s in Ball–Berry model was obtained by solving an equation connecting diffusion pathways of boundary layer and stomatal interface. h_a is relative humidity in the air. Humidity inside the intercellular space was assumed fully saturated. The resultant Equation (A30) is quadratic since $g_{s_{\mathrm{BB}}}$ has h_s in its component as defined in Equation (A26).

$$(h_s - h_a) g_b = (1 - h_s) g_{s_{\mathrm{BB}}} \tag{A30}$$

D_s in Medlyn model was obtained in a similar way. Water vapor pressure at the leaf surface (w_s), in the air (w_a), and in the intercellular space (w_i) were used instead of relative humidity values. The resultant Equation (A31) is quadratic since $g_{s_{\mathrm{MED}}}$ has D_s in its component as defined in Equation (A28). In an actual implementation, the equation was solved in terms of $\sqrt{D_s}$ and squared later to cope with a symbolic equation solver internally used by our framework.

$$(w_s - w_a) g_b = (w_i - w_s) g_{s_{\mathrm{MED}}} \tag{A31}$$

Appendix A.4. Energy Balance

Leaf temperature (T_l) can be different from air temperature (T_a) due to energy balancing on the leaf surface.

$$T_l = T_a + \Delta T \tag{A32}$$

The temperature difference (ΔT) is obtained by numerically solving the energy budget equation.

$$R_n - H - \lambda E = 0 \tag{A33}$$

The equation indicates that the net radiation absorbed by the leaf (R_n) should equal to the loss by sensible heat flux (H) and latent heat flux (λE), assuming no heat is stored in the leaf.

$$R_n = R_{sw} + R_{lw} \tag{A34}$$

$$R_{sw} = \alpha_s k I \tag{A35}$$

$$R_{lw} = 2\epsilon\sigma(T_{a_k}^4 - T_{l_k}^4) \tag{A36}$$

The absorbed net radiation (R_n) is composed of shortwave component driven by solar radiation (R_{sw}) and longwave component via thermal radiation (R_{lw}). Note that we assumed gas-exchange measured inside a small chamber and the temperature of chamber wall was equivalent to the surrounding air. α_s is absorption coefficient of the leaf for solar radiation and ϵ is thermal emissivity of the leaf. σ is Stefan-Boltzmann constant.

$$H = C_p g_h \Delta T \tag{A37}$$

For the sensible heat flux (H), C_p is specific heat of air and g_h is the convective heat conductance of the leaf surface.

$$E = g_v \Delta w \tag{A38}$$

$$g_v = \frac{1}{\frac{1}{g_s} + \frac{1}{g_b}} \tag{A39}$$

$$D = e_s[T_l] - e_a \tag{A40}$$

For the latent heat flux (λE), λ is the latent heat of vaporization for water. E is the transpiration rate calculated with leaf conductance (g_v) and vapor pressure gradient between leaf surface and the air (Δw). e_a is ambient vapor pressure of air. e_s is saturated vapor pressure at a given temperature (T).

$$e_s[T] = 0.611 \cdot \exp\left[\frac{17.502 \cdot T}{240.97 + T}\right] \tag{A41}$$

Appendix A.5. Coupling Submodels

The net photosynthetic rate (A_n) depends on mesophyll [CO_2] ($C_m \approx C_i$) through Equations (A2) and (A10). C_i depends on stomatal conductance (g_s) through Equation (A6). g_s then again depends on A_n through Equations (A26) and (A28), forming a cyclic dependency solved by an iterative numerical method. In the meantime, many parameters for A_n depends on temperature that the temperature of biochemical reaction site (T_l) should play an important role. Vapor pressure of intercellular space (pi) used for Medlyn stomatal conductance model can also change with T_l. The latent heat component of Equation (A33) solved for T_l is then driven by leaf conductance (g_v) which depends on g_s through Equation (A38).

Therefore, three submodels for photosynthesis, stomatal conductance, and energy balance are interdependent. We used a nested iterative procedure using the bisection method to solve this relation

numerically. For initial condition, each variable was given a sensible range of minimum and maximum values. C_i was assumed to be at least 0 µbar and lower than two times of C_a. ΔT, the difference between leaf temperature (T_l) and air temperature (T_a), was assumed in the range of -10 K and 10 K.

Appendix A.6. Implementation

An early version of the model was implemented in C++ and released as a sample of peer-reviewed publication of computer code [58]. Then, the model was translated, calibrated, and visualized with Cropbox framework [50] written in Julia programming language [17]. In this framework, a small component of the model is encapsulated into a structure called system and each system is a collection of variables described in a declarative form which closely resembles mathematical equations defined above and specifications of variables and parameters (Tables A1 and A2). The gas-exchange model was composed of 23 systems including a submodel for stomatal conductance (Figure A1).

The framework provides a number of unique types of variable declaration that can help hiding complexity of implementation details. For example, h_s in Equation (A30) is declared as a `solve` variable which is automatically expanded and solved in terms of symbolic algebra. ΔT in Equation (A32) in conjunction with Equation (A33) is declared as a `bisect` variable which would automatically generate necessary code to implement a nested iterative solver, as described in Appendix A.5. An optimal value of ΔT that satisfies $R_n = H + \lambda E$ as Equation (A33) would be found out by applying bisection method (Figure A2). Given Equation (A6) was also implemented as a `bisect` variable, the framework would analyze dependency between variables and generate proper code for nested structure.

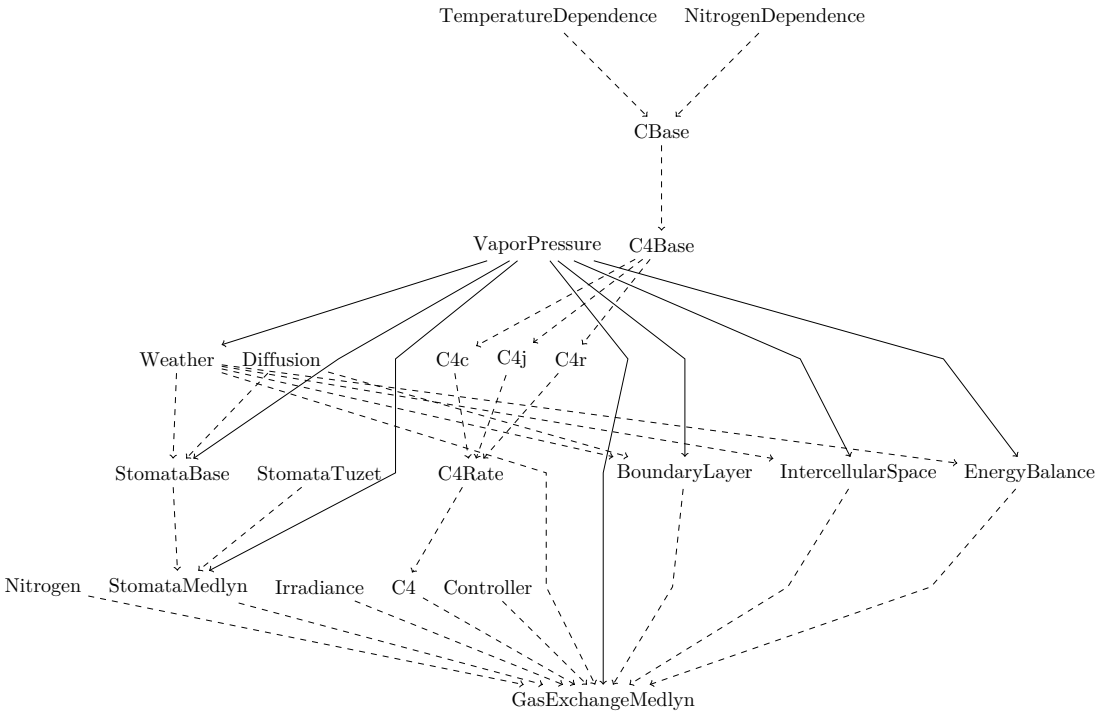

Figure A1. System diagram of the gas-exchange model (`GasExchangeMedlyn`) incorporating several submodels including Medlyn stomatal conductance model implemented on Cropbox framework. Solid arrow indicates 'has' relationship that the entity pointed out by the arrow owns the other entity and takes responsibility of state updates. Dashed arrow indicates 'is' relationship that the pointing entity becomes a trait of the other entity at the end.

```
@system EnergyBalance(Weather) begin
  ..
  ϵ: leaf_thermal_emissivity ⇒ 0.97 ~ preserve(parameter)
  σ: stefan_boltzmann_constant ⇒ u"σ" ~ preserve(u"W/m^2/K^4")
  λ: latent_heat_of_vaporization_at_25 ⇒ 44 ~ preserve(u"kJ/mol", parameter)
  Cp: specific_heat_of_air ⇒ 29.3 ~ preserve(u"J/mol/K", parameter)

  Δw(T, T_air, RH, ea=vp.ambient, es=vp.saturation): leaf_vapor_pressure_gradient ⇒ begin
      es(T) - ea(T_air, RH)
  end ~ track(u"kPa")
  E(gv, Δw): transpiration ⇒ gv*Δw ~ track(u"mmol/m^2/s")

  H(Cp, gh, ΔT): sensible_heat_flux ⇒ Cp*gh*ΔT ~ track(u"W/m^2")
  λE(λ, E): latent_heat_flux ⇒ λ*E ~ track(u"W/m^2")

  ΔT(R_net, H, λE): temperature_adjustment ⇒ begin
      R_net == H + λE
  end ~ bisect(lower=-10, upper=10, u"K", evalunit=u"W/m^2")

  T(T_air, ΔT): leaf_temperature ⇒ (T_air + ΔT) ~ track(u"°C")
  Tk(T): absolute_leaf_temperature ~ track(u"K")
end
```

Figure A2. Snippet of model code implementing energy balance process.

Note that all equations described in this section assume implicit units conversion and scaling which is a feature provided by Cropbox framework. For example, in Equation (A23), leaf width W was declared in 'cm' then automatically scaled to match the units of final product in 'm' that an actual code generated for calculating characteristic dimension was $d = 0.72\left(w \cdot 0.01\,\frac{\mathrm{m}}{\mathrm{cm}}\right)$.

Table A1. Variables declared in the model.

Symbol	Units	Description
C_4 Photosynthesis		
A_c	$\mu\mathrm{mol}_{CO_2}\,\mathrm{m}^{-2}\,\mathrm{s}^{-1}$	Rubisco-limited CO_2 assimilation rate
A_j	$\mu\mathrm{mol}_{CO_2}\,\mathrm{m}^{-2}\,\mathrm{s}^{-1}$	Electron transport-limited CO_2 assimilation rate
A_n	$\mu\mathrm{mol}_{CO_2}\,\mathrm{m}^{-2}\,\mathrm{s}^{-1}$	Net photosynthesis rate
C_a	µbar	Atmospheric CO_2 partial pressure
C_i	µbar	Intercellular CO_2 partial pressure
C_m	µbar	Mesophyll CO_2 partial pressure
J	$\mu\mathrm{mol}_{\mathrm{electrons}}\,\mathrm{m}^{-2}\,\mathrm{s}^{-1}$	Electron transport rate
J_{max}	$\mu\mathrm{mol}_{\mathrm{electrons}}\,\mathrm{m}^{-2}\,\mathrm{s}^{-1}$	Maximum rate of electron transport
k_N	-	Nitrogen dependence
k_{T_A}	-	Temperature dependence by Arrhenius equation
k_{T_Q}	-	Temperature dependence by Q_{10} function
k_{T_P}	-	Temperature dependence by a peaked function
K_c	µbar	Michaelis-Menton constant of Rubisco for CO_2
K_p	µbar	Michaelis-Menton constant of PEPC for CO_2
N	$\mathrm{g}\,\mathrm{m}^{-2}$	Leaf nitrogen content
N_p	%	Relative leaf nitrogen content assuming SLA = $200\,\mathrm{cm}^2\,\mathrm{g}^{-1}$
P_a	kPa	Atmospheric pressure
R_d	$\mu\mathrm{mol}_{CO_2}\,\mathrm{m}^{-2}\,\mathrm{s}^{-1}$	Mitochondrial respiration rate
r_{v_c}	$\mathrm{m}^2\,\mathrm{s}\,\mathrm{mol}_{CO_2}^{-1}\,\mathrm{bar}$	Total leaf resistance to CO_2
T_a	°C	Air temperature in Celsius
T_{a_k}	K	Air temperature in Kelvin
T_l	°C	Leaf temperature in Celsius
T_{l_k}	K	Leaf temperature in Kelvin
V_p	$\mu\mathrm{mol}_{CO_2}\,\mathrm{m}^{-2}\,\mathrm{s}^{-1}$	C_4 carboxylation rate
V_{pr}	$\mu\mathrm{mol}_{CO_2}\,\mathrm{m}^{-2}\,\mathrm{s}^{-1}$	PEP regeneration rate
V_{cmax}	$\mu\mathrm{mol}_{CO_2}\,\mathrm{m}^{-2}\,\mathrm{s}^{-1}$	Maximum rate of Rubisco carboxylation
$V_{p\mathrm{max}}$	$\mu\mathrm{mol}_{CO_2}\,\mathrm{m}^{-2}\,\mathrm{s}^{-1}$	Maximum rate of C_4 carboxylation
Boundary Layer		
d	m	Leaf characteristic dimension
g_b	$\mathrm{mol}_{H_2O}\,\mathrm{m}^{-2}\,\mathrm{s}^{-1}\,\mathrm{bar}^{-1}$	Boundary layer conductance to water vapor
g_h	$\mathrm{mmol}\,\mathrm{m}^{-2}\,\mathrm{s}^{-1}$	Leaf convective heat conductance in molar flux
g_H	$\mathrm{m}\,\mathrm{s}^{-1}$	Leaf convective heat conductance
r_{b_c}	$\mathrm{m}^2\,\mathrm{s}\,\mathrm{mol}_{CO_2}^{-1}\,\mathrm{bar}$	Boundary layer resistance to CO_2
u	$\mathrm{m}\,\mathrm{s}^{-1}$	Wind speed

Table A1. *Cont.*

Symbol	Units	Description
Irradiance		
I	$\mu mol_{quanta}\ m^{-2}\ s^{-1}$	Incident PAR
I_a	$\mu mol_{quanta}\ m^{-2}\ s^{-1}$	Absorbed PAR
I_2	$\mu mol_{quanta}\ m^{-2}\ s^{-1}$	Effective PAR
Stomatal Conductance		
D_s	kPa	Vapor pressure deficit at the leaf surface
f_{Ψ_v}	-	Water stress factor
g_s	$mol_{H_2O}\ m^{-2}\ s^{-1}\ bar^{-1}$	Stomatal conductance to water vapor
$g_{s_{BB}}$	$mol_{H_2O}\ m^{-2}\ s^{-1}\ bar^{-1}$	Stomatal conductance to water vapor from Ball–Berry model
$g_{s_{MED}}$	$mol_{H_2O}\ m^{-2}\ s^{-1}\ bar^{-1}$	Stomatal conductance to water vapor from Medlyn model
RH	%	Relative humidity of the air (0–100)
h_a	-	Relative humidity of the air (0–1)
h_s	-	Relative humidity at the leaf surface (0–1)
w_a	kPa	Water vapor pressure in the air
w_i	kPa	Water vapor pressure in the intercellular space
w_s	kPa	Water vapor pressure at the leaf surface
Ψ_v	MPa	Bulk leaf water potential
r_{s_c}	$m^2\ s\ mol^{-1}_{CO_2}\ bar$	Stomatal resistance to CO_2
Energy Balance		
Δw	kPa	Vapor pressure gradient between leaf surface and the air
e_a	kPa	Vapor pressure in the ambient air
e_s	kPa	Saturated vapor pressure
E	$mmol_{H_2O}\ m^{-2}\ s^{-1}$	Transpiration rate
g_v	$mol_{H_2O}\ m^{-2}\ s^{-1}\ bar^{-1}$	Total leaf conductance to water vapor
H	$W\ m^{-2}$	Sensible heat flux
λE	$W\ m^{-2}$	Latent heat flux
R_n	$W\ m^{-2}$	Net radiation absorbed
ΔT	K	Temperature difference between T_l and T_a

Input variables to the model (Table 1).

Appendix A.7. Workflow

A system implemented on Cropbox framework can be run by `simulate()` function supplied with an optional configuration. For instance, the coupled gas-exchange model with Medlyn stomatal conductance submodel (`GasExchangeMedlyn`) was run with a set of default parameters described in Tables 1 and A2 (Figure A3). `simulate()` function returns a result of simulation in a tabular data frame which can be further analyzed by various tools including own visualization methods provided by the framework. By default, the result contains values of all numerical variables declared in the controller system.

After testing models with initial parameters, calibration of four parameters, N_0, s, $g_{0_{MED}}$ and $g_{1_{MED}}$, as explained in Section 4.2 can be done by `calibrate()` function with a training dataset (Figure A4). In this example, we had two `target` variables in the dataset, `Photo` and `gs`, and wanted to compare them with `A_net` (A_n) and `gs` (g_s) estimated by the model. A percentage root mean square error (PRMSE) calculated from the difference between each set of variables was minimized by updating four parameters. The range of each parameter value is specified in `parameters` option.

Table A2. Parameters and constants used in the model.

Symbol	Value	Units	Description
C_4 Photosynthesis			
β	0.99	-	Sharpness of transition between A_c and A_j
E_{ac}	55.9 [59]	$\mathrm{kJ\,mol^{-1}}$	Activation energy for V_{cmax}
E_{aj}	32.8	$\mathrm{kJ\,mol^{-1}}$	Activation energy for J_{max}
E_{ap}	75.1	$\mathrm{kJ\,mol^{-1}}$	Activation energy for $V_{p\mathrm{max}}$
E_{ar}	39.8	$\mathrm{kJ\,mol^{-1}}$	Activation energy for R_d
g_{bs}	0.003 [12]	$\mathrm{mol_{CO_2}\,m^{-2}\,s^{-1}\,bar^{-1}}$	Bundle-sheath conductance to CO_2
H_j	220 [44]	$\mathrm{kJ\,mol^{-1}}$	Curvature parameter for J_{max}
$J_{\mathrm{max}_{25}}$	300	$\mathrm{\mu mol_{electrons}\,m^{-2}\,s^{-1}}$	Maximum rate of electron transport at 25 °C
$K_{c_{25}}$	650 [12]	µbar	Michaelis-Menton constant of Rubisco for CO_2 at 25 °C
$K_{p_{25}}$	80 [12]	µbar	Michaelis-Menton constant of PEPC for CO_2 at 25 °C
N_0	0.343	$\mathrm{g\,m^{-2}}$	Baseline leaf nitrogen content
R	8.314	$\mathrm{J\,K^{-1}\,mol^{-1}}$	Universal gas constant
$R_{d_{25}}$	2 [44]	$\mathrm{\mu mol_{CO_2}\,m^{-2}\,s^{-1}}$	Mitochondrial respiration rate at 25 °C
s	4.191	$\mathrm{m^2\,g^{-1}}$	Steepness of nitrogen response curve
S_j	702.6	$\mathrm{J\,mol^{-1}\,K}$	Entropy factor for J_{max}
θ	0.5	-	Sharpness of transition between light limitation and saturation
T_b	25	°C	Base temperature in Celsius
T_{b_k}	298.15	K	Base temperature in Kelvin
$V_{\mathrm{cmax}_{25}}$	50	$\mathrm{\mu mol_{CO_2}\,m^{-2}\,s^{-1}}$	Maximum rate of Rubisco carboxylation at 25 °C
$V_{p\mathrm{max}_{25}}$	70	$\mathrm{\mu mol_{CO_2}\,m^{-2}\,s^{-1}}$	Maximum rate of PEP carboxylation at 25 °C
$V_{pr_{25}}$	80 [12]	$\mathrm{\mu mol_{CO_2}\,m^{-2}\,s^{-1}}$	PEP regeneration rate at 25 °C
x	0.4 [12]	-	Partitioning factor of electron transport rate
Irradiance			
α	0.85 [54]	-	Leaf absorptance in PAR
δ	0.15 [55]	-	Leaf scattering factor
f	0.15 [55]	-	Leaf spectral correction factor
Boundary Layer			
$\mathcal{D}_w$	24.2	$\mathrm{mm^2\,s^{-1}}$	Diffusion coefficient for water vapor in air at 20 °C
$\mathcal{D}_c$	14.7	$\mathrm{mm^2\,s^{-1}}$	Diffusion coefficient for CO_2 in air at 20 °C
$\mathcal{D}_h$	21.5	$\mathrm{mm^2\,s^{-1}}$	Diffusion coefficient for heat (thermal diffusivity) in air at 20 °C
$\mathcal{D}_m$	15.1	$\mathrm{mm^2\,s^{-1}}$	Diffusion coefficient for momentum (kinematic viscosity) in air at 20 °C
W	10	cm	Leaf width
Stomatal Conductance			
$g0_{\mathrm{BB}}$	0.036	$\mathrm{mol_{H_2O}\,m^{-2}\,s^{-1}\,bar^{-1}}$	Lower bound of $g_{s_{\mathrm{BB}}}$
$g1_{\mathrm{BB}}$	2.792	-	Sensitivity of $g_{s_{\mathrm{BB}}}$
$g0_{\mathrm{MED}}$	0.031	$\mathrm{mol_{H_2O}\,m^{-2}\,s^{-1}\,bar^{-1}}$	Lower bound of $g_{s_{\mathrm{MED}}}$
$g1_{\mathrm{MED}}$	1.281	$\sqrt{\mathrm{kPa}}$	Sensitivity of $g_{s_{\mathrm{MED}}}$
Ψ_f	−2.0	MPa	Reference water potential
s_f	2.3 [23]	$\mathrm{MPa^{-1}}$	Sensitivity of water response
Energy Balance			
α_s	0.79 [60]	-	Radiation absorption coefficient of the leaf
C_p	29.3	$\mathrm{J\,mol^{-1}\,K^{-1}}$	Specific heat of air
ϵ	0.97 [53]	-	Leaf thermal emissivity
k	0.22	$\mathrm{J\,\mu mol^{-1}}$	Radiation conversion factor
λ	44	$\mathrm{kJ\,mol^{-1}}$	Latent heat of vaporization at 25 °C
σ	5.670×10^{-8}	$\mathrm{W\,m^{-2}\,K^{-4}}$	Stefan-Boltzmann constant

Parameter values calibrated in this paper. Parameter values calibrated with a dataset from [45].

```
c0 = (
    :StomataMedlyn ⇒ (g0 = 0.031, g1 = 1.281),
    :NitrogenDependence ⇒ (s = 4.191, N0 = 0.343),
    ..  # default configuration
)
r = simulate(GasExchangeMedlyn; config=c0)
```

Figure A3. Script for running a coupled gas-exchange model with Medlyn stomatal conductance submodel. Parameter values as listed in Table A2 are included in the baseline configuration `c0` used by `simulate()` function.

```
obs_df = .. # data frame contains gas exchange measurements
obs_C = .. # list of configurations for each measurement
c1 = calibrate(GasExchangeMedlyn, obs_df, obs_C;
    index = [:PARi ⇒ :PFD, :CO2S ⇒ :CO2, :RH_S ⇒ :RH, :Tair ⇒ :T_air, :Press ⇒ :P_air, :SPAD],
    target = [:Photo ⇒ :A_net, :gs],
    parameters = (
        :NitrogenDependence ⇒ (s=(0, 10), N0=(0, 1)),
        :StomataMedlyn ⇒ (g0=(0, 1), g1=(0, 10)),
    ),
    metric = :prmse,
    .. # other options
)
```

Figure A4. Script for calibrating parameters for the gas-exchange model. `index` option provides a mapping of variable names between a dataset and the model specification. `target` option indicates two variables, A_n and g_s, for which fitting errors are minimized. `parameters` option specifies a range of parameter values to be calibrated. A set of calibrated parameters are stored in a variable named `c1`.

Plotting model response in multiple ranges of criteria would require aggregation of results from models running multiple times with slightly different configuration. `visualize()` function takes care of a few common plotting scenarios in a simple interface. All figures in this paper were directly generated from the framework. For example, Figure 2b was generated by running `GasExchangeMedlyn` model with four levels of `RH` (RH) from 20 % to 80 % and plotting `gs` (g_s) against `Ci` (C_i) in lines (Figure A5). Each line of response was composed by changing `CO2` (C_a) in a range from 10 µbar to 1500 µbar at an interval of 10 µbar.

```
visualize(GasExchangeMedlyn; config=(c0, c1),
    x = :Ci, y = :gs,
    xstep = :Weather ⇒ :CO2 ⇒ 10:10:1500,
    group = :Weather ⇒ :RH ⇒ [80, 60, 40, 20],
    xlim = (0, 600), ylim = (0, 1), legendpos = (0.8, 0),
    kind = :line
)
```

Figure A5. Script for generating Figure 2b. `visualize()` function internally runs `simulate()` and render a plot using the output. Note that a configuration used here is the baseline `c0` partially overridden by the calibrated `c1`. `x` and `y` options specify variables used for two axes of the plot. `xstep` option provides a range of value to compose a single curve, indicating atmospheric CO_2 concentration (C_a) is ranged from 10 µbar to 1500 µbar. `group` option provides a group of treatments to render multiple curves, indicating four levels of relative humidity (RH) are used. `xlim` option sets the visible range of C_i limited from 0 µbar to 600 µbar and `ylim` option sets the range of g_s from 0 to 1 $\mathrm{mol_{H_2O}\,m^{-2}\,s^{-1}\,bar^{-1}}$. `kind` option for plot type can be either `:line` or `:scatter`.

A Jupyter notebook containing source code of the model with calibration datasets and scripts for producing figures presented in this paper is available at https://github.com/cropbox/plants2020.

Appendix B. Calibration of SPAD Measurements

Our experimental dataset used in calibration had SPAD measurements as a proxy to leaf nitrogen content. A small number of samples were separately collected from direct measurement of leaf nitrogen content and then used to derive a relationship between SPAD measurement and leaf nitrogen content. A quadratic equation in the form of $N = ax^2 + bx + c$ was fitted for leaf nitrogen content (N) and SPAD measurement (x = SPAD) where $a = 0.0004$, $b = 0.012$, and $c = 0$ with $R^2 = 0.92$ (Figure A6).

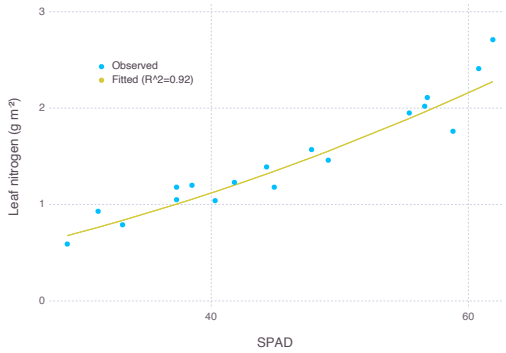

Figure A6. Fitting SPAD measurement to leaf nitrogen content (N). N was fitted by a quadratic equation $N = 0.0004x^2 + 0.012x$ for 18 samples of SPAD measurement (x = SPAD) with $R^2 = 0.92$.

Appendix C. Sensitivity of Nitrogen Parameters

The sensitivity of parameters related to nitrogen dependence was obtained by calculating net photosynthesis rate (A_n) with a range of values for the parameter in question, while keeping other parameters unchanged (Figure A7). For reference, N_0 was 0.371 and 0.315, and s was 4.470 and 3.912, for BB and MED, respectively. Baseline leaf nitrogen content (N_0) barely had an impact on A_n with its range from 0.2 g m^{-2} to 0.5 g m^{-2}. Sensitivity of nitrogen response curve (s) did not make a large difference either within the range of calibrated parameter values. For example, two sets of N_0 and s mentioned above resulted into less than 1 % difference in A_n at 400 µmol m^{-2} s^{-1} of ambient CO_2 level. Therefore we assumed the difference between nitrogen parameter values we obtained from calibration for BB and MED were negligible and safe to pool them together for one unified set of parameters. The averaged out values for N_0 and s used in the rest of simulation was 0.343 and 4.191 (Table A2).

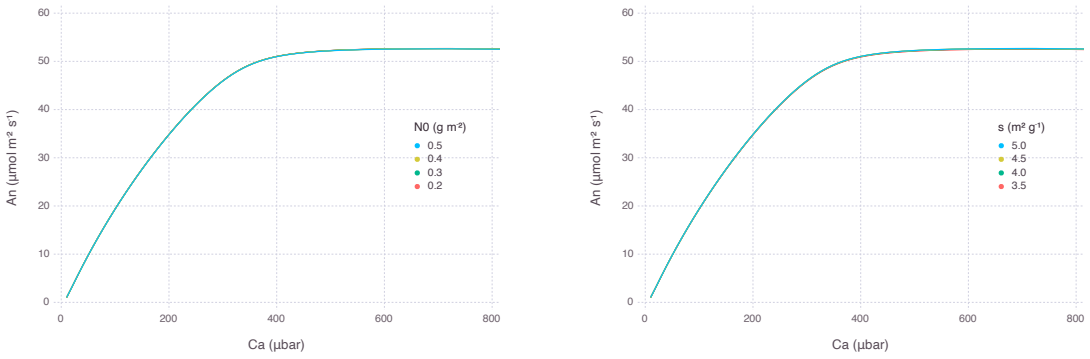

(**a**) Baseline leaf nitrogen content (N_0)

(**b**) steepness of nitrogen response (s)

Figure A7. Sensitivity of parameters related to nitrogen dependence. The coupled gas-exchange model with Medlyn stomatal conductance model was used for testing. Air temperature (T_a) was 32 °C, irradiance (I) was 2000 µmol$_{quanta}$ m^{-2} s^{-1}, and relative humidity (RH) was 66 %.

Appendix D. Parameters for Transgenic Plants

A few parameters were derived to replicate a wide range of temperature response of transgenic plants with reduced amounts of Rubisco reported by Kubien et al. [39]. We mostly used the same values for variables and parameters identified in the paper, except $J_{max_{25}}$, which was not mentioned but needed adjustments to replicate original curves (Table A3). Measured values of A_n, g_s, and C_i under three treatments were digitized from their Figure 1. WT indicates wild type, while AR1 and AR2 refers to mutants treated with anti-Rubisco antibody to have Rubisco content reduced to 49 % and 32 %, respectively.

Table A3. Variables and parameters for replicating experiment by Kubien et al. [39].

Symbol	Value	Units	Description
Input variables			
C_a	370	µbar	Atmospheric CO_2 partial pressure
D	12	mbar	Vapor pressure deficit of the air (converted to RH)
I	1500	$\mu mol_{quanta}\ m^{-2}\ s^{-1}$	Incident PAR
Shared parameters			
$g0_{BB}$	0.138	$mol_{H_2O}\ m^{-2}\ s^{-1}\ bar^{-1}$	Lower bound of $g_{s_{BB}}$
$g0_{MED}$	0.138	$mol_{H_2O}\ m^{-2}\ s^{-1}\ bar^{-1}$	Lower bound of $g_{s_{MED}}$
Parameters for WT			
E_{ac}	56.1	$kJ\ mol^{-1}$	Activation energy for V_{cmax}
E_{ap}	71.6	$kJ\ mol^{-1}$	Activation energy for V_{pmax}
$J_{max_{25}}$	300	$\mu mol_{electrons}\ m^{-2}\ s^{-1}$	Maximum rate of electron transport at 25 °C
$V_{cmax_{25}}$	51.48	$\mu mol_{CO_2}\ m^{-2}\ s^{-1}$	Maximum rate of Rubisco carboxylation at 25 °C
$V_{pmax_{25}}$	159.9	$\mu mol_{CO_2}\ m^{-2}\ s^{-1}$	Maximum rate of PEP carboxylation at 25 °C
Parameters for AR1			
E_{ac}	57.0	$kJ\ mol^{-1}$	Activation energy for V_{cmax}
E_{ap}	69.4	$kJ\ mol^{-1}$	Activation energy for V_{pmax}
$J_{max_{25}}$	240	$\mu mol_{electrons}\ m^{-2}\ s^{-1}$	Maximum rate of electron transport at 25 °C
$V_{cmax_{25}}$	24.7	$\mu mol_{CO_2}\ m^{-2}\ s^{-1}$	Maximum rate of Rubisco carboxylation at 25 °C
$V_{pmax_{25}}$	186.3	$\mu mol_{CO_2}\ m^{-2}\ s^{-1}$	Maximum rate of PEP carboxylation at 25 °C
Parameters for AR2			
E_{ac}	59.3	$kJ\ mol^{-1}$	Activation energy for V_{cmax}
E_{ap}	74.0	$kJ\ mol^{-1}$	Activation energy for V_{pmax}
$J_{max_{25}}$	120	$\mu mol_{electrons}\ m^{-2}\ s^{-1}$	Maximum rate of electron transport at 25 °C
$V_{cmax_{25}}$	15.54	$\mu mol_{CO_2}\ m^{-2}\ s^{-1}$	Maximum rate of Rubisco carboxylation at 25 °C
$V_{pmax_{25}}$	146.9	$\mu mol_{CO_2}\ m^{-2}\ s^{-1}$	Maximum rate of PEP carboxylation at 25 °C

Minimum g_s observed in the dataset. Scaled to the ratio of maximum A_n for each treatment to make up missing information.

References

1. Kim, S.H.; Hsiao, J.; Kinmonth-Schultz, H. Advances and improvements in modeling plant processes. In *Advances in Crop Modelling for a Sustainable Agriculture*; Boote, K., Ed.; Burleigh Dodds Science Publishing: London, UK, 2019; pp. 3–43.
2. Yin, X.; Struik, P. C_3 and C_4 photosynthesis models: An overview from the perspective of crop modelling. *NJAS-Wagen. J. Life Sci.* **2009**, *57*, 27–38. [CrossRef]
3. Wu, A.; Song, Y.; van Oosterom, E.J.; Hammer, G.L. Connecting biochemical photosynthesis models with crop models to support crop improvement. *Front. Plant Sci.* **2016**, *7*, 1518. [CrossRef]
4. Collatz, G.J.; Ball, J.T.; Grivet, C.; Berry, J.A. Physiological and environmental regulation of stomatal conductance, photosynthesis and transpiration: A model that includes a laminar boundary layer. *Agric. For. Meteorol.* **1991**, *54*, 107–136. [CrossRef]
5. Leuning, R. A critical appraisal of a combined stomatal-photosynthesis model for C_3 plants. *Plant Cell Environ.* **1995**, *18*, 339–355. [CrossRef]
6. Nikolov, N.T.; Massman, W.J.; Schoettle, A.W. Coupling biochemical and biophysical processes at the leaf level: An equilibrium photosynthesis model for leaves of C_3 plants. *Ecol. Model.* **1995**, *80*, 205–235. [CrossRef]
7. Kim, S.H.; Lieth, J.H. A Coupled Model of Photosynthesis, Stomatal Conductance and Transpiration for a Rose Leaf (*Rosa Hybrida* L.). *Ann. Bot.* **2003**, *91*, 771–781. [CrossRef] [PubMed]
8. Tuzet, A.; Perrier, A.; Leuning, R. A coupled model of stomatal conductance, photosynthesis and transpiration. *Plant Cell Environ.* **2003**, *26*, 1097–1116. [CrossRef]
9. Farquhar, G.D.; von Caemmerer, S.; Berry, J.A. A biochemical model of photosynthetic CO_2 assimilation in leaves of C_3 species. *Planta* **1980**, *149*, 78–90. [CrossRef]
10. Ball, J.T.; Woodrow, I.E.; Berry, J.A. A model predicting stomatal conductance and its contribution to the control of photosynthesis under different environmental conditions. In *Progress in Photosynthesis Research*; Biggens, J., Ed.; Springer: Dordrecht, The Netherlands, 1987; pp. 221–224.

11. Medlyn, B.E.; Duursma, R.A.; Eamus, D.; Ellsworth, D.S.; Prentice, I.C.; Barton, C.V.M.; Crous, K.Y.; de Angelis, P.; Freeman, M.; Wingate, L. Reconciling the optimal and empirical approaches to modelling stomatal conductance. *Glob. Chang. Biol.* **2011**, *17*, 2134–2144. [CrossRef]
12. Von Caemmerer, S. *Biochemical Models of Leaf Photosynthesis*; CSIRO Publishing: Clayton, Australia, 2000; pp. 91–100.
13. Collatz, G.; Ribas-Carbo, M.; Berry, J. Coupled photosynthesis-stomatal conductance model for leaves of C_4 plants. *Funct. Plant Biol.* **1992**, *19*, 519–538. [CrossRef]
14. Sellers, P.; Randall, D.; Collatz, G.; Berry, J.; Field, C.; Dazlich, D.; Zhang, C.; Collelo, G.; Bounoua, L. A revised land surface parameterization (SiB2) for atmospheric GCMS. Part I: Model formulation. *J. Clim.* **1996**, *9*, 676–705. [CrossRef]
15. Duursma, R.A. Plantecophys — An R package for analysing and modelling leaf gas exchange data. *PLoS ONE* **2015**, *10*, 1–13. [CrossRef] [PubMed]
16. Hartzell, S.; Bartlett, M.S.; Porporato, A. Unified representation of the C_3, C_4, and CAM photosynthetic pathways with the Photo3 model. *Ecol. Model.* **2018**, *384*, 173–187. [CrossRef]
17. Bezanson, J.; Edelman, A.; Karpinski, S.; Shah, V.B. Julia: A fresh approach to numerical computing. *SIAM Rev.* **2017**, *59*, 65–98. [CrossRef]
18. Sinclair, T.R.; Rufty, T.W. Nitrogen and water resources commonly limit crop yield increases, not necessarily plant genetics. *Glob. Food Secur.* **2012**, *1*, 94–98. [CrossRef]
19. Medlyn, B.E.; Badeck, F.W.; de Pury, D.G.G.; Barton, C.V.M.; Broadmeadow, M.; Ceulemans, R.; de Angelis, P.; Forstreuter, M.; Jach, M.E.; Kellomäki, S.; et al. Effects of elevated [CO_2] on photosynthesis in European forest species: A meta-analysis of model parameters. *Plant Cell Environ.* **1999**, *22*, 1475–1495. [CrossRef]
20. Vos, J.; van der Putten, P.E.L.; Birch, C.J. Effect of nitrogen supply on leaf appearance, leaf growth, leaf nitrogen economy and photosynthetic capacity in maize (*Zea Mays* L.). *Field Crop. Res.* **2005**, *93*, 64–73. [CrossRef]
21. Kattge, J.; Knorr, W.; Raddatz, T.; Wirth, C. Quantifying photosynthetic capacity and its relationship to leaf nitrogen content for global-scale terrestrial biosphere models. *Glob. Chang. Biol.* **2009**, *15*, 976–991. [CrossRef]
22. Dewar, R.C. The Ball–Berry–Leuning and Tardieu–Davies stomatal models: synthesis and extension within a spatially aggregated picture of guard cell function. *Plant Cell Environ.* **2002**, *25*, 1383–1398. [CrossRef]
23. Yang, Y.; Kim, S.H.; Timlin, D.J.; Fleisher, D.H.; Quebedeaux, B.; Reddy, V.R. Simulating canopy transpiration and photosynthesis of corn plants under contrasting water regimes using a coupled model. *Trans. ASABE* **2009**, *52*, 1011–1024. [CrossRef]
24. Franks, P.J.; Berry, J.A.; Lombardozzi, D.L.; Bonan, G.B. Stomatal function across temporal and spatial scales: Deep-time trends, land–atmosphere coupling and global models. *Plant Physiol.* **2017**, *174*, 583–602. [CrossRef] [PubMed]
25. Franks, P.J.; Bonan, G.B.; Berry, J.A.; Lombardozzi, D.L.; Holbrook, N.M.; Herold, N.; Oleson, K.W. Comparing optimal and empirical stomatal conductance models for application in Earth system models. *Glob. Chang. Biol.* **2018**, *24*, 5708–5723. [CrossRef] [PubMed]
26. Duursma, R.A.; Blackman, C.J.; Lopéz, R.; Martin-StPaul, N.K.; Cochard, H.; Medlyn, B.E. On the minimum leaf conductance: Its role in models of plant water use, and ecological and environmental controls. *New Phytol.* **2019**, *221*, 693–705. [CrossRef] [PubMed]
27. Hsiao, J.; Swann, A.L.; Kim, S.H. Maize yield under a changing climate: The hidden role of vapor pressure deficit. *Agric. For. Meteorol.* **2019**, *279*, 107692. [CrossRef]
28. Hsiao, T.C.; Jackson, R.B. Interactive effects of water stress and elevated CO_2 on growth, photosynthesis, and water use efficiency. In *Carbon Dioxide and Environmental Stress*; Luo, Y.; Mooney, H.A., Eds.; Academic Press: San Diego, CA, USA, 1999; pp. 3–31.
29. Ghannoum, O. C_4 photosynthesis and water stress. *Ann. Bot.* **2008**, *10*, 635–644. [CrossRef] [PubMed]
30. Markelz, R.J.C.; Strellner, R.S.; Leakey, A.D.B. Impairment of C_4 photosynthesis by drought is exacerbated by limiting nitrogen and ameliorated by elevated [CO_2] in maize. *J. Exp. Bot.* **2011**, *62*, 3235–3246. [CrossRef] [PubMed]
31. Xu, Z.; Shimizu, H.; Yagasaki, Y.; Ito, S.; Zheng, Y.; Zhou, G. Interactive effects of elevated CO_2, drought, and warming on plants. *J. Plant Growth Regul.* **2013**, *32*, 692–707. [CrossRef]

32. Manderscheid, R.; Erbs, M.; Weigel, H.J. Interactive effects of free-air CO_2 enrichment and drought stress on maize growth. *Eur. J. Agron.* **2014**, *52*, 11–21. [CrossRef]
33. Zong, Y.; Shangguan, Z. Nitrogen deficiency limited the improvement of photosynthesis in maize by elevated CO_2 under drought. *J. Integr. Agric.* **2014**, *13*, 73–81. [CrossRef]
34. Van der Kooi, C.J.; Reich, M.; Löw, M.; De Kok, L.J.; Tausz, M. Growth and yield stimulation under elevated CO_2 and drought: A meta-analysis on crops. *Environ. Exp. Bot.* **2016**, *122*, 150–157. [CrossRef]
35. Leakey, A.D.; Uribelarrea, M.; Ainsworth, E.A.; Naidu, S.L.; Rogers, A.; Ort, D.R.; Long, S.P. Photosynthesis, productivity, and yield of maize are not affected by open-air elevation of CO_2 concentration in the absence of drought. *Plant Physiol.* **2006**, *140*, 779–790. [CrossRef] [PubMed]
36. Morgan, J.A. Interaction of water supply and N in wheat. *Plant Physiol.* **1984**, *76*, 112–117. [PubMed]
37. Shangguan, Z.; Shao, M.; Dyckmans, J. Effects of nitrogen nutrition and water deficit on net photosynthetic rate and chlorophyll fluorescence in winter wheat. *J. Plant Physiol.* **2000**, *156*, 46–51. [CrossRef]
38. Roth, J.A.; Ciampitti, I.A.; Vyn, T.J. Physiological evaluations of recent drought-tolerant maize hybrids at varying stress levels. *Agron. J.* **2013**, *105*, 1129–1141. [CrossRef]
39. Kubien, D.S.; von Caemmerer, S.; Furbank, R.T.; Sage, R.F. C_4 photosynthesis at low temperature. A study using transgenic plants with reduced amounts of Rubisco. *Plant Physiol.* **2003**, *132*, 1577–1585. [CrossRef]
40. Crafts-Brandner, S.J.; Salvucci, M.E. Sensitivity of photosynthesis in a C_4 Plant, maize, to heat stress. *Plant Physiol.* **2002**, *129*, 1773–1780. [CrossRef]
41. Urban, J.; Ingwers, M.W.; McGuire, M.A.; Teskey, R.O. Increase in leaf temperature opens stomata and decouples net photosynthesis from stomatal conductance in *Pinus Taeda Populus Deltoides X Nigra*.*J. Exp. Bot.* **2017**, *68*, 1757–1767. [CrossRef]
42. Peak, D.; Mott, K.A. A new, vapour-phase mechanism for stomatal responses to humidity and temperature. *Plant Cell Environ.* **2011**, *34*, 162–178. [CrossRef]
43. Buckley, T.N.; Mott, K.A. Modelling stomatal conductance in response to environmental factors. *Plant Cell Environ.* **2013**, *36*, 1691–1699. [CrossRef]
44. Kim, S.H.; Gitz, D.C.; Sicher, R.C.; Baker, J.T.; Timlin, D.J.; Reddy, V.R. Temperature dependence of growth, development, and photosynthesis in maize under elevated CO_2. *Environ. Exp. Bot.* **2007**, *61*, 224–236. [CrossRef]
45. Kim, S.H.; Yang, Y.; Timlin, D.J.; Fleisher, D.H.; Dathe, A.; Reddy, V.R.; Staver, K. Modeling temperature responses of leaf growth, development, and biomass in maize with MAIZSIM. *Agron. J.* **2012**, *104*, 1523–1537. [CrossRef]
46. Storn, R.; Price, K. Differential evolution – A simple and efficient heuristic for global optimization over continuous spaces. *J. Glob. Optim.* **1997**, *11*, 341–359. [CrossRef]
47. Kim, S.H.; Sicher, R.C.; Bae, H.; Gitz, D.C.; Baker, J.T.; Timlin, D.J.; Reddy, V.R. Canopy photosynthesis, evapotranspiration, leaf nitrogen, and transcription profiles of maize in response to CO_2 enrichment. *Glob. Chang. Biol.* **2006**, *12*, 588–600. [CrossRef]
48. Willmott, C.J.; Robeson, S.M.; Matsuura, K. A refined index of model performance. *Int. J. Climatol.* **2012**, *32*, 2088–2094. [CrossRef]
49. Nash, J.; Sutcliffe, J. River flow forecasting through conceptual models part I – A discussion of principles. *J. Hydrol.* **1970**, *10*, 282–290. [CrossRef]
50. Available online: https://github.com/tomyun/Cropbox.jl (accessed on 12 October 2020).
51. Kirschbaum, M.U.F. The sensitivity of C_3 photosynthesis to increasing CO_2 concentration: A theoretical analysis of its dependence on temperature and background CO_2 concentration. *Plant Cell Environ.* **1994**, *17*, 747–754. [CrossRef]
52. Buckley, T.N.; Mott, K.A.; Farquhar, G.D. A hydromechanical and biochemical model of stomatal conductance. *Plant Cell Environ.* **2003**, *26*, 1767–1785. [CrossRef]
53. Campbell, G.S.; Norman, J. *An Introduction to Environmental Biophysics*, 2nd ed.; Springer: New York, NY, USA, 1998; pp. 106, 109, 136, 244.
54. Jones, H.G. *Plants and Microclimate: A Quantitative Approach to Environmental Plant Physiology*, 3rd ed.; Cambridge University Press: Cambridge, UK, 2013; pp. 28, 59, 345.
55. De Pury, D.G.G.; Farquhar, G.D. Simple scaling of photosynthesis from leaves to canopies without the errors of big-leaf models. *Plant Cell Environ.* **1997**, *20*, 537–557. [CrossRef]

56. Medlyn, B.E.; Loustau, D.; Delzon, S. Temperature response of parameters of a biochemically based model of photosynthesis. I. Seasonal changes in mature maritime pine (*Pinus Pinaster* Ait.). *Plant Cell Environ.* **2002**, *25*, 1155–1165. [CrossRef]
57. Monteith, J.L.; Unsworth, M.H. *Principles of Environmental Physics: Plants, Animals, and the Atmosphere*, 4th ed.; Academic Press: Cambridge, MA, USA, 2014; pp. 31–33, 151–157, 379.
58. Timlin, D.; David, O.; Green, T.R.; Fleisher, D.H.; Kim, S.H.; Ahuja, L.R. Proposed standards for peer-reviewed publication of computer code. *Agron. J.* **2016**, *108*, 1782–1786. [CrossRef]
59. Sage, R.F. Variation in the kcat of Rubisco in C_3 and C_4 plants and some implications for photosynthetic performance at high and low temperature. *J. Exp. Bot.* **2002**, *53*, 609–620. [CrossRef] [PubMed]
60. Earl, H.J.; Tollenaar, M. Maize leaf absorptance of photosynthetically active radiation and its estimation using a chlorophyll meter. *Crop Sci.* **1997**, *37*, 436–440. [CrossRef]